Analyst

CRITICAL REVIEW

View Article Online
View Journal | View Issue

Cite this: *Analyst*, 2018, **143**, 2971

Advancements in microfluidic technologies for isolation and early detection of circulating cancer-related biomarkers

Ankit Rana,[a] Yuqian Zhang [a] and Leyla Esfandiari *[a,b]

Received 4th December 2017,
Accepted 27th April 2018

DOI: 10.1039/c7an01965c

rsc.li/analyst

Early stage detection of cancer is essential for the improved long-term survival of patients. Currently, costly, extensively complex and invasive procedures, such as surgical tissue biopsies, are used for cancer screening. Thus, over the past few decades, advancements in microfluidics and lab-on-a-chip approaches have been made to develop minimally invasive and miniaturized platforms to identify and segregate circulating cancer biomarkers such as exosomes, circulating tumor cells (CTCs) and cell-free DNA (cfDNA) from body fluids. Our study presents a comprehensive overview of all such microfluidics based approaches for point-of-care cancer diagnostics, which have proven to require significantly reduced sample volumes with cost effective and minimally invasive criteria. We have also discussed the need for integrated and more efficient devices to further advance these technologies to be suitable for liquid biopsy in the clinical settings.

1. Introduction

Cancer is among the leading causes of morbidity and mortality. In 2012, the World Health Organization reported more than 14.1 million new cancer cases worldwide and 8.2 million cancer-related deaths.[1] Although it is well accepted that early diagnosis is the only certain way to defeat cancer, to this day even in developed countries, the majority of cancer diagnostics rely on invasive tissue biopsies or on bulky and expensive imaging instrumentation.[2] Commonly, the patients forsake screening due to the nature of these methods. Recently, there have been significant efforts in the identification and isolation of cancer-related biomarkers in body fluids such as circulating tumor cells (CTCs), small extracellular vesicles (exosomes), proteins, and cell-free DNAs (cfDNA)[3] depicted in Fig. 1. Detection methods based on circulating biomarkers, known as liquid

[a]*Department of Electrical Engineering and Computer Science, College of Engineering and Applied Sciences, University of Cincinnati, Cincinnati, Ohio 45221, USA*
[b]*Department of Biomedical Engineering, College of Engineering and Applied Sciences, University of Cincinnati, Cincinnati, Ohio 45221, USA.*
E-mail: esfandla@ucmail.uc.edu

Ankit Rana

Ankit is a graduate student of Electrical Engineering at the University of Cincinnati. His research focuses on the study of electrokinetic effects in a nanopore based biosensor device. He is interested in the development of minimally invasive in vitro *diagnostic (IVD) platforms that are fast and economical while being robust. His MS work has been towards studying the effect of forces such as electroosmosis and dielectrophoresis at the nanoscale, which he studied with finite element simulations of the biosensor setup in use.*

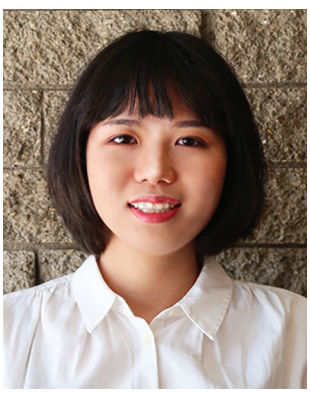

Yuqian Zhang

Yuqian Zhang received her bachelor's degree in Renewable Energy Materials and Device from the University of Electronic Science and Technology of China in 2015. Currently, she is a Ph.D. student at the University of Cincinnati in Electrical Engineering. Her research interests include nanopore-based sensing, nucleic acid detection and circulating biomarker sorting for medical diagnostics.

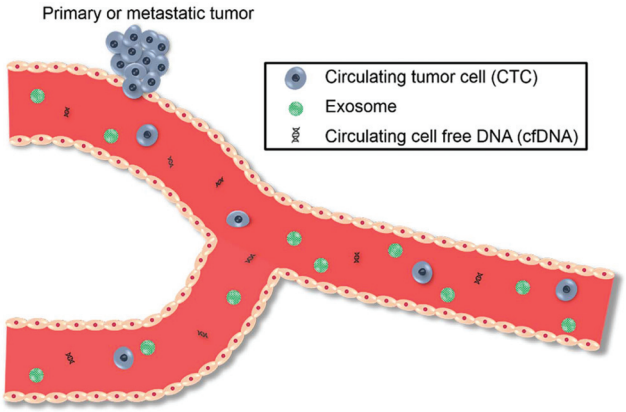

Fig. 1 Circulating biomarkers in cancer.

biopsies, are less invasive and can serve as better representatives of the primary and metastatic sites compared to the traditional tissue biopsies.[4] However, in the typical clinical approaches, a considerable fraction of blood is required since the detection efficiency of biomarkers present in smaller volume remains low.[5] Therefore, there is a clear and pressing need for the development of point-of-care, minimally invasive and highly sensitive diagnostic technologies that allow patients to routinely screen for early signs of cancer.[6] In recent years, much work has been done specifically to reduce the required sample volume and enhance the sensitivity of the detection by leveraging from micro-/nano-scale technologies; and hence, excellent review articles and book chapters regarding the isolation of CTCs and exosomes have been published.[7–14] For instance, a critical review by Issadore's group has covered the novel nano-/micro-device based solutions for the isolation of circulating biomarkers with emphasis on the detection of exosomes and recognizing their clinical relevance in cancer.[15] Jung's group has presented a minireview summarizing the commercially available technologies for the isolation and enrichment of the circulating biomarkers.[5] Although these articles provided exquisite insights into the commercially available and nano-/micro-scaled technologies, there are a very limited number of review articles that comprehensively discuss the state-of-the-art microfluidic technologies for the isolation and detection of the three major circulating biomarkers from body fluids. Here, our review discusses the advanced microfluidic devices and their principles employed in the separation and detection of circulating CTCs, cfDNA and exosomes in a more comprehensive way. Also, the need for more efficient methods to further advance these technologies to be suitable for liquid biopsy in clinical settings has been provided.

Leyla Esfandiari

Dr Leyla Esfandiari is an assistant professor with dual appointment in Electrical Engineering and Biomedical Engineering at the University of Cincinnati, USA. She is the principal investigator of the Integrative BioSensing Laboratory with the main focus on design and development of nano-/micro-scaled bioanalytical tools and microfluidic devices for medical and environmental applications. Dr Esfandiari completed her doctoral degree in bioengineering from the University of California Los Angeles (UCLA) in 2014. She has won numerous awards including the William E. Restemeyer Teaching Excellence Award, UC Faculty Development Award, UCLA Unrestricted Fellowship, UCI Kleist Fellowship, the NSF Fellowship for Cell Mechanics, and the Boeing Scholarship.

2. Circulating tumor cell (CTC) isolation techniques

2.1 CTCs as circulating biomarkers

Studies related to circulating tumor cells (CTCs) have shown that these cells hold a primary role in metastatic spread[16] and their successful detection at early stages has given hope to cure such a life-threatening disease by providing vital clues regarding cancer metastasis. However, CTCs are extremely rare in the bloodstream and their co-existence with a large number of white blood cells (WBCs), erythrocytes and a myriad of other biomolecules makes their detection technically challenging.[17] Also, the CTCs' large morphological variability and size heterogeneity make their identification and characterization a daunting task.[16,17] Additionally, CTCs are prone to damage from the stress induced during the staining step or the shear-stress due to the course of flow in channels.[18] This poses a challenge for the extraction of a viable amount from the samples. Most notably, since CTCs are rare species, a large quantity of blood sample (~5–10 mL) is needed to be drawn from patients for successful detection.[16]

2.2 Conventional methods for the isolation of CTCs

Over the course of time, a plethora of CTC isolation and detection techniques have been implemented[19–24] which can be broadly categorized as: (a) cytometric, which relies on the intensities of the emitted scattered light as fluorescently labelled tumor cells pass through a laser spot;[25] (b) immunomagnetic separation, an approach primarily based on the expression of the EpCAM lineage marker which has remained a benchmark isolation method;[26] CellSearch, a conventionally used device, and the only FDA approved approach to detect CTCs in whole blood, has been an immuno-magnetic segregation standard;[27] this method relies on the efficiency of the EpCAM epitope expressed in epithelium and fatal tumors; despite its popularity, it has shown great variability in terms of sensitivity and specificity;[28] and (c) morphological-based separation, assays that provide a way to differentiate epithelial

tumor cells from leukocytes which are relatively smaller in size. This approach is subject to the alterations in shape and size of the tumor cells in the process and hence, it is not highly efficient.[29]

Although the conventional CTC screening techniques provide essential information regarding these rare cells, long processing times and significant variations amongst isolation methods have added to the inconsistencies, making them unreliable for clinical studies.[16,17] Thus, more efficient and consistent systems are required for reliable isolation and characterization of these cells with high viability rates and purity. Additionally, ensuring that the least amount of stress is applied on the cells during the process and high reproducibility of results are critical for highly accurate diagnosis and prognosis.

2.3 Isolation of CTCs using microfluidic technologies

Miniaturization of the devices reduces the sufficient volume of blood for the isolation of CTCs and the analysis time compared to the conventional methods. In this section, we comprehensively review a wide range of the state-of-the-art microfluidic techniques aimed at optimizing the isolation of CTCs from blood samples by size and physical properties including dielectric nature and immunoaffinity binding.

2.3.1 Micro-filtration. The commonly used separation method is the size-based approach. Since cancer cells are larger in diameter than both leukocytes and erythrocytes, they can be sorted out by the micro-filtration method. Zheng *et al.* presented a three-dimensional microfilter system to enrich human breast adenocarcinoma cells (MCF7) from diluted blood samples.[30] The device was fabricated with two layers of Parylene membrane with a gap and pores accurately fabricated by the photolithography technique to trap cancer cells and keep them viable for further downstream analysis. The results showed that the device could enrich viable CTCs from ~1 mL of whole blood with a recovery rate of ~86% within five minutes. Using another simple passive micro-well device, Tan *et al.* isolated the spiked cancer cells MCF7, human breast adenocarcinoma (MDA-MB-231) cells, and human colon adenocarcinoma (HT-29) cells from diluted blood.[31] The micro-device incorporated a pre-filtration and multiple arrays of crescent-shaped wells to prevent cell clumps and realize the separation. The platform successfully achieved significant CTC isolation with 80% efficiency and 0.7 mL h^{-1} throughput under 5 kPa input pressure while preserving the viability of the cells. However, in the case of large sample volume, the major limitation of most filter-based devices is clogging.[32] To address this shortcoming, Kim *et al.* devised a lab-on-a-disc platform which integrated a track-etched polycarbonate membrane with 8 μm diameter pores with a fluid-assisted separation technology (FAST) to isolate CTCs from the unprocessed whole blood of cancer patients.[33] The FAST disc was composed of three independent filtration units, each consisting of three chambers for sample loading, filtration and waste storage. Whole blood was loaded into the sample chamber and was gently pushed into the filtration chamber in which the blood was pumped radially outwards as the disc spun. The larger CTCs were captured by the membrane while smaller hematopoietic cells passed through the membrane and to the waste chamber. The FAST disc showed 20 seconds filtration of 3 mL whole blood with the recovery rate up to ~96%. Further, Qin *et al.* used the resettable cell trap mechanism in which a two layered polydimethylsiloxane (PDMS) structure was fabricated in which the upper PDMS layer served as the flow channel whereas the other worked as the sample-filled control channel.[34] The flow channel consisted of microstructured pockets to trap target cells. The two layers were separated by a pneumatically controlled flexible diaphragm, which could constrict or relax, thus enabling the capture and release of the target cell species, respectively. The group tested the device with blood samples collected from 22 patients with metastatic castrate-resistant prostate cancer and it was shown that it could recover greater than 5 CTCs in 82% of the patients from 7.5 mL of blood (diluted twice) in around 10 minutes.

Besides single tumor cell isolation, it is essential to separate the multicellular groups (metastasis) from the bloodstream. With this objective, Sarioglu *et al.* developed a microchip technology to capture the metastasis from unprocessed whole blood.[35] The microchip took advantage of the larger size and the strength of cell–cell junctions of CTC clusters and captured them in specialized bifurcation traps under low-shear stress conditions, thus conserving cell viability (Fig. 2). It was shown that the device could capture cell clusters from 30% of patients with melanoma, 40% of patients with breast cancer and 31% of patients with prostate cancer.

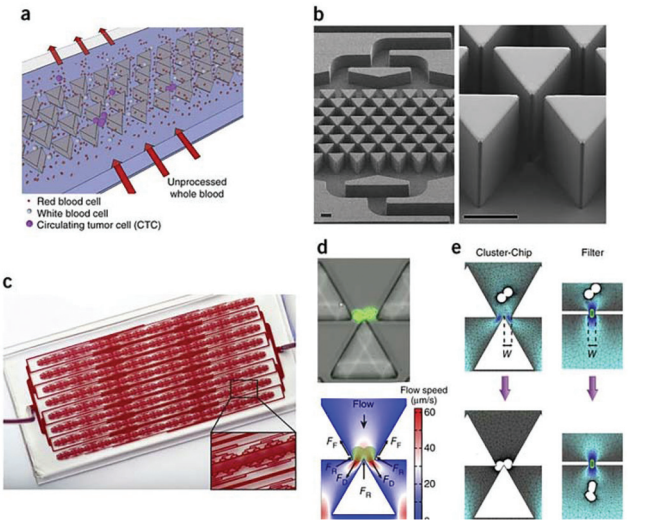

Fig. 2 Cluster-chip design and operation.[35] (a) The capture of CTC clusters from unprocessed whole blood while the single cells flow through. (b) SEM images showing the triangular features that serve as consecutive cluster traps and a magnified image of a cluster trap. Both scale bars at 60 μm. (c) Actual image of a working cluster-chip. (d) A two-cell human prostate adenocarcinoma cluster captured on the chip (top) and a schematic elucidation of the acting forces responsible for this capture (bottom). (e) Finite-element analysis comparing the cell cluster dynamics in the chip (left) and in a filter with one equivalent opening (right).

Although being label-free and providing a rapid filtration process are significant advantages of micro-filter separation methods, they are prone to clogging when handling large volumes of blood samples. The heterogeneous size distribution, deformability and clustering of cell population makes it difficult to set a cut-off size and to attain a high purity of desired CTCs.

2.3.2 Electrokinetic isolation. The dielectric property of cells relies on their cellular composition including their membrane capacitance, cytosolic conductivity and diameters, which can be used for their classification. Among the electrokinetics based devices, dielectrophoresis is broadly used for the manipulation of charged molecules, including cells, nucleic acids and exosomes. The dielectrophoretic (DEP) force can arise from the non-uniform electric field gradient and is based on the relative permittivity of the particles to the medium. The direction of this force could be towards the high field gradient (positive DEP), or away from the high field gradient (negative DEP).[22] The unique dielectric property of CTCs provides a promising opportunity to separate them from the other cell populations utilizing the DEP scheme. In a study by Chou *et al.*, an optically induced dielectrophoretic (ODEP)-based cell separation technique was integrated into a microfluidic device for CTC isolation after an initial size selective membrane filtration process.[36] This microfluidic system comprised of four concurrent layers: a PDMS layer, an indium tin-oxide (ITO) glass substrate, an adhesive tape and an ITO coated photoconductive material layer (top to bottom). Four rectangular photoactive zones termed 'light bar arrays' (40 μm wide) were fabricated in the photoconductive layer. These served as virtual cell-filters for the target creating four isolation zones arranged in a cascading manner. By applying an alternating-current (AC) between the two ITO glass layers, a uniform electric field polarized the biological species. Further, controllable light images originating from a commercially available projector were used as a source illuminating the light bar arrays. This led to electron–hole pair excitation in the photoconductive layer forming four non-uniform field regions accompanied by a noticeable voltage drop in the solution. Thus, the previously polarized species were manipulated with the locally generated non-uniform electric field in the arrays. Further, due to the variable width of the microchannels, a flow velocity control was established facilitating target isolation. Under the optimal ODEP manipulating conditions with 5 volts peak to peak applied field at 100 kHz, the method showed its ability to isolate CTCs (PC-3 cancer cells) with ~95% purity.

Electrical impedance spectroscopy (EIS) is another electrokinetic-based technology for the characterization of cells based on their dielectric properties and at single-cell resolution.[37,38] Frazier's group proposed a microelectrical impedance spectroscopy (μ-EIS) system integrated with a magnetophoretic microseparator, to isolate CTCs from blood sample. The μ-EIS measurements showed that the human breast cancer cell lines at different pathological stages can be distinguished from the normal human breast tissue cell line by analyzing the impedance magnitude and phase.[39] Further, to quantify the tumor cell population, the same group designed a pressure-driven isolation device to trap a single tumor cell in microfabricated cavities and measure its electrical impedance with the μEIS system, operable over a frequency range of 100 kHz to 3 MHz.[40] Based on the impedance data gathered at 100 kHz frequency, the membrane capacitance for the cells was computed. This analysis showed a 4–19% capacitance decrease for the carcinoma bearing cell-lines compared to the healthy cell line.

As illustrated in these studies, the electrokinetic-based separation is expected to be more translatable into the clinical settings. However, challenges with target specificity, complicated device fabrication and an operational design that often requires the use of a high electric field and high aspect ratio microstructures prevent their implementation in clinical applications.[41–44]

2.3.3 Inertial microfluidic approach. In microfluidics the inertial forces become significant where the balance between the wall effect and the shear gradient lift forces provides a controllable net force that can separate particles based on their specific size and deformability. Manipulation of the forces is mainly carried out by changing the channel dimensions or introducing a new fluid inlet. A pioneering work in the field of inertial microfluidics by Papautsky's group demonstrated focusing of particles at distinct locations in a spiral microchannel.[45] A combination of dominant inertial forces and the Dean rotational force in the curvilinear microchannel was the underlying sorting mechanism in their system. The device was 90% efficient and showed great cell viability when utilized to separate neuroblastoma and glioma cells. This technique served as an integral first stage spiral component of another highly efficient two-stage inertial microfluidic device developed by Lee's group.[46] The device could selectively focus small cells (RBCs or smaller prostate cancer cells) from a heterogeneous cell population in two steps. In the first step, the net lift force on the cells interacted with the curvature induced Dean drag forces. These forces reach an equilibrium closer to the inner walls of the channel providing focusing positions for the larger cells (>18 μm). This helped in removing the entities of a non-target nature from the blood samples. In the next step, the extracted sample was enforced into an active lateral cavity acoustic transducer (LCAT) where a gas–liquid interface was acoustically actuated leading to the generation of microstreaming flows. These oscillatory vortices selectively segregated larger particles towards the center of the vortex while the smaller species were farther outwards and were flown away with the rest of the fluid. A 10× diluted blood sample was flown at a rate of 1.1 mL min^{-1} through the device providing a ~44 000× enriched output target cell (RBC) volume of ~50 μL in 5 minutes. Another platform presented by Di Carlo's group, was centered on blood-analysis aimed at isolating CTCs for breast and lung cancer prognosis.[47] The approach was to merge the micro-scale vortices and inertial focusing for high-purity isolation of CTCs from blood. Cells with different sizes were flown through the channel and were pushed apart from each other due to the induced wall and shear forces applied to

them. Initially, the group methodically altered the channel size and flow rate parameters to maximize the efficiency and purity while confirming the cell viability. It has been shown that approximately 25–51 CTCs were captured per 7.5 mL of breast cancer patient blood and about 23–317 CTCs per 7.5 mL of lung cancer patient blood. The complete procedure took approximately 20 minutes, resulting in a varying 57–94% purity. To further improve the device, a Deformability Cytometry (DC) system was integrated with the device to enable one-step capture, release and enumeration of CTCs. Once the CTCs were captured in the vortices and the impurities were washed away, the CTCs were rapidly released to the DC section for deformability analyses. This comprehensive technology reached a detection accuracy of 93.8% and allowed complete enumeration of CTCs from 10 mL of blood sample within 1 hour.

Another inertial device with new channel geometry for CTC isolation was put forth by Warkiani *et al.* The group devised an innovative spiral microfluidic device having a trapezoidal cross-section shape for the entrapment of CTCs from 7.5 mL of blood sample volume.[48] By means of a trapezoidal cross-section instead of a customary rectangular cross-section, the location of the Dean Vortex core was changed to accomplish better segregation. Smaller hematologic constituents were confined in the Dean vortices askew towards the outer channel walls and ultimately were detached at the outer outlet, while the bigger CTCs equilibrated near the inner channel wall and were gathered from the inner outlet. A separation of more than 80% of the tested cancer cell lines (MCF-7, T24 and MDA-MB-231) with very high purity was attained under 8 minutes.

Park *et al.* introduced another unique label-free approach to capture viable circulating tumor cells directly from unprocessed whole blood samples.[49] The method relied on the varying deformability of cells as they passed through constriction zones under a continuous oscillatory flow. The cells were flown through a matrix of tapered micrometer scale constrictions and because of the oscillatory flow, a ratcheting motion was produced which led the tumor cells, erythrocytes and leukocytes in different flow paths despite their nearly identical dimensions. The device was capable of gathering more than 90% of the cancer cells from 2 mL of unprocessed whole blood to achieve 10^4-fold enrichment of tumor cells compared to leukocytes. Also, in the cases where CTCs and leukocytes are similar sized (*e.g.* prostate cancer samples), the device performed deformability based isolation providing a 25× yield compared to the conventional cell-size based 'CellSearch' approach.

The inertial micro-devices provide a label-free separation without relying on an external electric or magnetic field; these devices have emerged as a straightforward and easy to incorporate approach for a lab-on-a-chip design. Such an integrated microchip can perform both CTC capture and downstream analysis thereafter. However, the inertial systems have their own shortcomings. For instance, once fabricated, making design alterations in a device is difficult and therefore, one needs to make new devices for each application. Furthermore, there exists a particle concentration limit, meaning that after some time, due to the particle accumulation in the channel, the steric interaction within particles or the target species hinders the isolation process.[50]

2.3.4 Immunoaffinity-based isolation. Among the isolation techniques, the immunoaffinity-based approach has been the most popular for sorting CTCs due to better specificity and purity outcomes. Generally, this method is based on the specific binding of CTCs by their surface markers with the immobilized antibodies on microstructures in the microfluidic channels while other cells and debris are flushed out of the device. Recently, Soper's group has developed a microfluidic device which is capable of selective isolation of CTCs from a blood sample.[51] In this approach, unpurified blood at a rate of 1 mL per 37 min was flown through a series of fifty-one high aspect-ratio channels replicated in Polymethyl methacrylate (PMMA) conjugated with monoclonal antibodies (mAB) against EpCAM expression in CTCs of epithelial origin. This focused the sample into a smaller volume (~190 nL). As the CTCs were captured in the channels, they were moved towards the quantification stage. The cells were released using trypsin and traversed through the platinum detection electrodes serving as a conductivity sensor. As they crossed, positive spikes were observed in the conductance trace across the electrodes signifying the isolated tumor cells, following the Coulter-counter principle.[52] A tumor cell output of 10–250 CTCs from 1 mL of whole blood samples taken from breast cancer patients was attained in under 40 minutes. Later, they improved the capture efficiency to 97% with the use of sinusoidal shaped narrower channels (35 μm wide). The easy fabrication procedure, rapid operation and favorable isolation results made this device a promising tool for clinical applications.

Another pioneered immunoaffinity based approach was devised by Nagrath *et al.* that could address the low yield and purity of isolated tumor cells using conventional methods.[53] At the core of this technique was the idea of maximizing cell–micropost contact in the flow path which would result in a higher capture efficiency. Their approach was independent of pre-dilution or pre-labelling of whole blood sample and could conduct isolation in a single step. The microfluidic platform was termed, 'the CTC-chip' and was capable of selectively isolating viable CTCs from 2.7 mL whole blood flown at a rate of 1–2 mL h^{-1}. The target CTCs interacted with antibody EpCAM-coated micro-posts which enabled the sensing of CTCs with 99% efficiency (115/116 patient samples) and a yield ranging from 5 to 1281 CTCs per mL of the sample with 50% purity (two orders higher than the existing technologies).

In another study, Kang *et al.* designed a device which used a combination of microfluidic and micromagnetic operations to isolate, sense and culture tumor cells from crude samples.[54] The device was primarily made of PDMS and was comprised of a microfluidic architecture with one primary channel and one redundant collection channel and rows of dead-end side cavities for tumor cell assortment. The cell isolation was carried out by EpCAM antibody-coated magnetic microbeads with

2.8 μm diameters under a fluid flow rate of 1.2 mL h^{-1}. The separation efficiency of about 90% was achieved when 1 mL of blood extracted from a wild type mouse was spiked with 2 to 80 breast cancer cells. The performance of the device over a period of 20 weeks was analyzed, which showed an increase in the metastatic tumor cells count with time. One of the major challenges with the above techniques is the minimal interaction of the cells with the immobilized antibodies due to the axial direction of the flow with respect to the channels. To overcome this challenge, Stott *et al.* described a high-throughput microfluidic mixing means, the herringbone-chip (HB-Chip), to improve CTC isolation.[55] Through the HB-chip, approximately 4 mL of blood was driven by pressure at a rate of 1.2 mL h^{-1} with a median of 63 circulating cells being captured from every milliliter of blood. Cell capture was confirmed by a defined count of cancer cells spiked into control blood samples. Further, the clinical viability of the system was established using samples from patients with prostate cancer. In 14 out of 15 patients (~93%), samples with metastasis and tumor-specific exon translocation were successfully recognized.

Evolving this method, Park *et al.* incorporated a nanostructured substrate and a thiolated ligand-exchange reaction onto a microfluidic chip with herringbone structures.[56] To enhance the isolation sensitivity, instead of conjugating the antibodies on a flat silicon oxide surface, the anti-EpCAM-coated gold nanoparticles were assembled on the chip surface resulting in the increase of the surface area for CTC binding. Meanwhile, the metal–thiol interaction could easily be disrupted by the presence of excess thiol molecules resulting in the release of cancer cells from the surface for downstream analysis. In this study, 3 mL of blood containing cancer cell ranging from 10 to 1000 cells per mL was flown at a rate of 1 mL h^{-1} and the results showed a linear relationship between spiked cells and captured cells with an efficiency of ~80 to 96%. Meanwhile, for ultralow concentration isolation, 5 cells per mL of breast cancer cells (MDA-MB-231) and prostate cancer cell lines (PC3) were studied under the same flow rate and the average capture efficiency was reported to be 68% and 72%, respectively. Also, the device showed a great release efficiency of ~90%.

While the presented immunoaffinity approaches had high purity and efficiency outcome, the majority of them have been limited to cells of epithelial origin. Antibody–EpCAM binding is known to introduce cytotoxicity.[57] Also, due to epithelial-to-mesenchymal transition (EMT), CTCs are known to lose their EpCAM expression levels and evade the detection process.[58] To avoid EpCAM binding, a complementary approach aimed at depleting the WBCs by using antibodies against leukocytes and thereby isolating the tumor cells was devised by Karabacak *et al.* through a microfluidic CTC-iChip.[59] This approach comprised of a novel EpCAM-free design and catered to the tumor cells which would typically lose EpCAM expression during the labelling processes due to the dynamic epithelial mesenchymal transition.[60] The CTC-iChip consisted of two components termed as chip 1 and chip 2, respectively. The chip 1 component performed deterministic lateral displacement (DLD)[61] for the separation of nucleated cells from whole blood. It comprised of a serially arranged filter array and a micropost array capable of deflecting particles with diameters greater than 4 μm and separating them from the main suspension. The cells which were not labeled don't deflect and follow the streamlines leading them to the physical end of the device. At this stage, RBCs, platelets and the free beads were removed from the flow. The chip 2 component carried out inertial focusing[62] for precise positioning of the filtered cells in a single line. Having been focused, the serially aligned bead-labelled WBCs and unlabeled CTCs undergo sensitive immunomagnetic segregation by means of a high magnetic field gradient which pushes the bead labeled WBCs to the center of the channel while the CTCs don't feel the effect of the gradient.[63] The device produced a high throughput rate of up to 10^7 cells per s accounting for 97% output efficiency in cell-separation with a whole blood sample processed at a rate of 8 mL h^{-1} (Fig. 3).

An alternative to the EpCAM antibodies to isolate CTCs was the use of aptamers as probe molecules. Aptamers are oligonucleotides that specifically bind to a target molecule and have been used as a substitute to antibodies due to their high stability, easier release and higher specificity towards smaller molecules.[64,65] In this light, Phillips *et al.* reported a DNA aptamer-based CTC enrichment microchip and demonstrated the feasibility of rare cell entrapment without any pretreatment.[66] The DNA aptamer was used against a T-cell acute lymphocytic

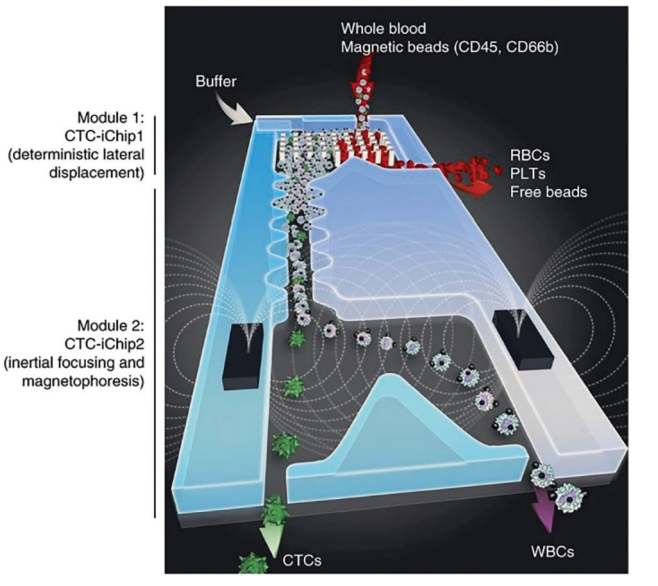

Fig. 3 A schematic of the CTC-iChip[59] that uses three different principles for WBC and CTC enrichment. At the top, continuous lateral displacement for the size-selective separation of white blood cells and tumor cells from whole blood samples can be seen with the use of deflections from micropost arrays. Further down the channel, the cells undergo inertial focusing into a straight line which is fed into the magnetophoresis section at the bottom, eventually segregating tumor cells and leukocytes.

leukemia cell line, which is a proven effective cultured precursor target for aptamer selection.[67] This approach achieved a capture yield of 80% and a purity of 97% when the diluted cell samples were flown at a rate below 200 nL s^{-1}. Later, Sheng *et al.* reported the development of a micropillar-based microfluidic device that was capable of proficiently segregating tumor cells from unprocessed 1 mL whole blood samples.[68] In this approach, high-affinity aptamers were used as a substitute for antibodies for colorectal cancer cell isolation and were immobilized *via* avidin–biotin interactions on a glass slide that consisted of more than 59 000 micropillars. Further, the group used the device for targeting the leukemia cells in a mixture of 1000 human acute lymphoblastic leukemia and 10^6 Ramos cells seeded in 1 mL of buffer solution. With permutations in device geometry and flow rates, the aptamer and target interaction were optimized and thus, the results yielded a capture efficiency of approximately 95% with a purity of 81% at the optimum flow rate of 600 nL s^{-1}. The device further addressed the problem of low throughput capability of conventional microfluidic devices by processing 1 mL of blood in less than 30 minutes with a cell viability of ~93%. Although the method was promising, it required complex fabrication procedures to produce glass micropillar geometries on the substrate.

An interesting scheme emerged based on the use of magnetic sensors for the detection of CTCs from a complex biological matrix. Exploiting this principle, Issadore *et al.* presented an innovative microfluidic chip-based sensor that could detect the immuno-magnetically labelled CTCs in 7.5 mL of whole blood with minimal sample preparation.[69] The sensor was named the MicroHall (μHall) platform owing to its capability of detecting cells labelled with magnetic nanoparticles (MNPs). A channel overlying 2 × 4 arrays of 8 μHall sensors was placed in a uniform magnetic field, which enabled each cell to pass over at least two of the eight μHall components on the course of its flow. Voltage output signals were recorded as the cells traversed through the channel, which were relative to the MNP density per cell and facilitated a benchmark for molecular analysis. The capability of this sensor to detect a single cell from the larger population of other blood matrix constituents was significant and the overall assay time was 2.5 hours. Later, Muluneh and Issadore established the capability of integration of several magnetic sensor-chips with a solitary microfluidic device to provide a method for parallelized processing of samples on the chip.[70] They quoted magnetic cytometry towards detection of rare cells as a key area for its application, which is limited in terms of the sample flow velocity and can measure only one cell at a time through a channel.

Based on a similar approach, Kwak *et al.* developed a magnetic force gradient microfluidic device for the selective isolation and characterization of a heterogeneous subpopulation of CTCs.[71] The magnetic nanoparticles were functionalized with anti-EpCAM and the tagged CTCs were derived to different locations along the device due to the magnetic force differences resulting from CTC EpCAM expression levels. The EpCAM positive CTCs were trapped at a lower magnetic intensity area in the first half of the chip while the EpCAM negative ones were gathered at higher magnetic field regions in the latter half. The experiment showed that 95.7% of EpCAM positive cells and 79.3% of EpCAM negative cells were isolated by the chip. Also, the device was capable of isolating CTC populations in 3 mL of a sample in 1 hour and distinguish their heterogeneity, which aided in metastasis evaluation of the cancer. However, the main drawback of the immuno-magnetic isolation method is the irreversible binding of magnetic beads to the surface of CTCs. To address this issue, Xiao *et al.* developed an effective way to capture and release CTCs using Fe_3O_4@MnO_2 nanoparticles conjugated with anti-EpCAM.[72] MnO_2 could be disrupted by extremely low oxalic acid at room temperature resulting in easy detachment of captured cells and thus, the downstream analyses of the cells. The capture efficiency of the system was reported to be 83% with the release efficiency of 57% and cell viability of approximately 70%. Furthermore to avoid using the EpCAM antibody, Lee *et al.* introduced an integrated microfluidic device to negatively exclude the background cells using magnetic nanoparticles (MNPs) instead of driving CTCs with a magnetic force.[73] The chip contained a micromixer to generate multi-vortices to increase the interaction between CD45-antibody modified MNPs and white blood cells. All the isolation process was carried out in one-step on the chip and thus, the loss of CTCs was minimized. As the magnet-coated white blood cells were trapped by the magnetic field, CTCs were left in the channel for subsequent identification by immunohistochemical staining or molecular analysis.

The majority of the techniques mentioned in this section were based on the isolation of CTCs by their specific biomarkers and are summarized in Table 1. There is no doubt that the isolation based on the surface markers have provided high purity outcomes; however, the drawbacks were also evident at the same time due to the heterogeneous properties of CTCs. The EpCAM expression levels may vary in a CTC population and thereby lead to lower yield and loss of valuable information. Besides, the release of captured CTCs usually required the addition of specific reagents which could result in cell death and the loss of viable CTCs for downstream analysis.

3. Cell-free DNA (cfDNA) isolation techniques

3.1 Cell-free DNA as circulating biomarkers

In blood, there are two kinds of circulating DNAs—the one that is associated with lymphocytes and cell-free DNAs (cfDNA). The studies with cfDNA, particularly carcinoma progression and its stage introduced variations, have been exceedingly promising. For instance, in cancer patients, especially gastric and colorectal carcinoma, the high concentration levels of cfDNA were correlated with cancer progression.[74] Furthermore, cfDNA as a circulating biomarker has proven to be more informative, specific and accurate than protein biomarkers.[75,76] The ease of extraction without harming its physi-

Table 1 Summary of CTC isolation techniques

Platform	Separation method	Sample	Throughput	Volume	Recovery rate	Advantage	Ref.
Micro-filter	Size	Diluted whole blood	~0.25 mL min^{-1}	~1 mL	95.9%	Improved recovery rate, cost-effective	30
	Size	Diluted blood	0.7 mL h^{-1}	5 mL	>80%	Label-free, easy to operate	31
	Size	Unprocessed whole blood	>3 mL min^{-1}	3 mL	96%	Clog-free, fast, highly sensitive	33
	Size	Diluted whole blood	0.75 mL min^{-1}	7.5 mL	82%	Clog-free	34
	Size	Unprocessed whole blood/MDA-MB-231 clusters	2.5 mL h^{-1}	1–10 mL	30–40%	Label-free	35
DEP based	Electric field	Cell suspension in EDTA treated sucrose with stained PC-3 cancer cells	0.4 μL min^{-1}	10 μL	94.9%	Label-free, clog-free	36
Inertia	Inertial force	Whole blood	1.1 mL min^{-1}	50 μL	>91%	High purity	46
	Inertial force	Whole blood	0.375 mL min^{-1}	7.5 mL	>75%	Applicable to different cancer types, cost-effective, rapid	47
	Inertial force	Whole blood	~1 mL min^{-1}	7.5 mL	>80%	Ultra-fast, label-free	48
	Inertial force	Unprocessed whole blood	1 mL h^{-1}	2 mL	>90%	Label-free	49
Immuno-magnetic affinity based	EpCAM antibody	Unpurified whole blood	>1.5 mL h^{-1}	>1 mL	>97%	Easy to fabricate, rapid	51
	EpCAM antibody	Whole blood	1.2 mL h^{-1}	1 mL	90%	High throughput, easy to fabricate	54
	EpCAM antibody	Whole blood	1.5–2.5 mL h^{-1}	5 mL	93%	High throughput	55
	EpCAM antibody	Whole blood	1 mL h^{-1}	3 mL	96.4% for ~1000 PC3 cells per mL	Enhanced capture efficiency and recovery	56
	EpCAM antibody, inertial, magnetophoretic forces	Whole blood	8 mL h^{-1}	8 mL	97%	Highest throughput	59
	EpCAM antibody	Whole blood	~10^7 cells per min	7.5 mL	10 out of 10	Cost-effective, single cell detection	69
	EpCAM antibody, magnetophoretic forces	Peripheral blood	3 mL h^{-1}	3 mL	95.7%	Rapid	71
	EpCAM antibody, magnetophoretic forces	PBS buffer	~35 min	1 mL	80%–86%	High throughput, good cell viability	72
	CD-45 antibody, inertial, magnetophoretic forces	Whole blood	>200 μL min^{-1}	>5 mL	94.2%	Single step enrichment, reduced CTC loss	73
Aptamer based	Aptamers–target cell binding	PBS	0.5 mL h^{-1}	50 μL	80%	High purity (97%), rapid	66
	Aptamers–target cell binding	Unprocessed whole blood	600 nL s^{-1}	1 mL	~95%	Good purity (~81%), rapid	68

cal condition adds to its utility.[77] Several kinds of gene mutations that are associated with different tumors have been observed structurally in cfDNA including point mutations, losses of heterozygosity, DNA hypermethylations and microsatellite instabilities.[78–81] Often these modifications were alike to the ones from primary tumor tissue, which further supports their feasibility as circulating cancer biomarkers.

3.2 Conventional method for isolation of cfDNA

In terms of isolation techniques, in-house procedures based around real-time PCR quantification have been the conventional and commercially available means. These methods have remained devoid of a standardized set of pre-analytical phases in terms of sample collection, its storage, and the choice of a processing medium between plasma and serum,[82] to name a few. Besides amplification reliant approaches, commercially available kits that use organic compounds (phenol/chloroform) and employ the ion-exchange binding of DNA for extraction have been introduced.[77,83] However, these methods have proven to be costly, time consuming, and require large sample volumes.[84] Thus, there is a need for more efficient and robust cfDNA isolation techniques, possibly by means of novel microfluidic devices that can further be developed as a POC diagnostic standard.

3.2 Isolation of cfDNA using microfluidics

Microfluidic based digital PCR has been utilized for the detection and analysis of cfDNA with high accuracy and precision

compared to the DNA purification kits.[85] However, PCR-oriented approaches have been known to be labor intensive, expensive, and time consuming. Thus, recently, DEP based microfluidics have been developed for cfDNA detection. For instance, Sonnenberg *et al.* used a DEP device to isolate cfDNA from 25 μL samples of plasma from chronic lymphocytic leukemia (CLL) patients under an AC field with a cut off frequency of 10 kHz while using a 11 volts peak-to-peak sinusoidal signal within a total processing time of 10 minutes.[86] The approach involved the separation of cfDNA into high-field DEP region posts, where other blood matrix constituents were captured at low-field regions and eventually omitted by means of a fluidic wash (Fig. 4). Subsequently, concentrated cfDNA was sensed by optical measurements and quantified by PCR and the next generation sequencing method. The group further used an approach based on the same principle but this time beginning with larger sample volumes of 300 μL of blood, in which the cfDNA was separated in 10 minutes from the plasma.[87] The device was employed to further detect and isolate cfDNA from T7 (mCherry) bacteriophage virus from blood samples of chronic lymphocytic leukemia (CLL) patients and human mitochondria.[88] As an improvement over the conventional means,[89–92] this DEP process is only comprised of two steps and can be completed within 10 minutes using 20 μL of blood at an operational frequency of 10 kHz and 20 volts.

In another study by Yang *et al.*, a microfluidic device was designed with the objective of distinguishing nucleic acids in whole blood samples under 10 minutes.[93] The device could extract cfDNA from blood without any enrichment or extensive preparation and it was comprised of a sample channel, an accumulation channel and a pair of electrodes. A DC electric field of approximately 20 volts was applied to move the fluorescently labelled cfDNA molecules from the sample channel to the collection channel while crossing a centrally located intersectional area at which an optical sensor assembly carried out the quantification measurements.

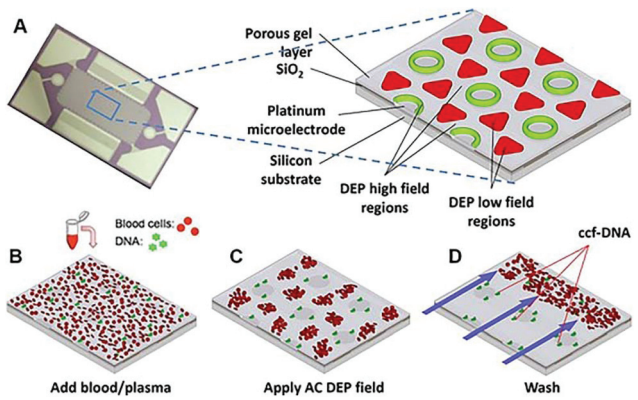

Fig. 4 The DEP microarray device operation developed by Heller and group for segregating cf-DNA from blood and plasma.[87] (a) The AC bias based electrokinetic microarray device (chip) used with an expanded view of the device material composition. (b) The microarray device with whole blood (red) and fluorescent DNA (green); (c) the usage of the AC electric field leading to the fluorescent DNA (green) to be concentrated in the high-field regions, while the blood cells (red) move into the low-field regions between the microelectrodes; and (d) a fluidic wash removing the blood cells from the microarray while DNA stays on the electrodes.

Electrokinetics based isolation devices have typically been utilized with a lower conductivity sample medium, and are attained after a series of processing steps such as precipitation and suspension. With higher conductive body fluid samples such as plasma, blood and serum, the operational voltages and the cut-off frequencies tend to be larger. Microarray devices have been able to perform isolation under these conditions; however, they undergo damage at the uncoated platinum electrodes due to electrochemical degradation. To address this issue, an electrokinetics based isolation study was carried out by Heller's group, which experimented with two design setups while being able to isolate nucleosomes and cell-free DNA from body fluids.[94] With a parallel wire setup, under low-conductance conditions (10^{-4} S m^{-1}), fluorescent beads were successfully isolated. However, with high-conductance conditions, high electrothermal flow (ETF) was observed, which led to electrochemical degradation of the electrodes. To overcome this problem, the group conducted experiments with a planar microarray design and was able to isolate beads without the effect of ETF at a higher conductivity of approximately 1 S m^{-1}. This planar device was successfully utilized to isolate cfDNA from an un-diluted plasma sample. In this approach, 25 μL plasma sample was loaded to the chip with an applied AC field of 14 Vpp at 15 kHz. CfDNA and nucleosomes were isolated under 20 minutes and were later detected directly on the microarray *via* incubation by means of the AlexaFluor 594-conjugated secondary antibody in red fluorescence.

The importance of microstructures in DEP based devices in terms of the surface area for biomolecular interaction and constructs for their effective entrapment is immense. This aspect was explored by Cho's group, which developed a novel scheme to efficiently capture and isolate cfDNA using a reusable nanostructured polypyrrole (Ppy) nanochip.[95] They took advantage of the reversible changes in the electrochemical reduction–oxidation (redox) state of Ppy to control the surface charge of the material, and thereby were able to adsorb or release cfDNA fragments from the chip. The device had a 3D array of Ppy/gold nanowires at its core, which provided unique constructs that could serve as a reservoir for the efficient capture of cfDNA. This design showed improved performance in DNA capture and release with an efficiency of ~90% when the sample concentration of DNA was more than 1 ng mL^{-1} and 50% with a lowered DNA concentration of 10 pg mL^{-1}. The excellent performance of the Ppy chip for the isolation of cfDNA may serve as valuable diagnostic and prognostic strategies.

Although the discussed electrokinetics based microfluidic schemes for the isolation of cfDNA are simple, rapid and relatively cost-effective, the key challenge is to maintain the purity and yield of the extracted cfDNA from blood samples while complying with the reusability criteria. The DEP based designs required complicated fabrication procedures and staining

steps posing a serious question regarding the viability of the method as a large-scale POC solution. Furthermore, the short half-life of cfDNA in the physiological condition poses challenges in their extraction and their detection sensitivity and specificity. Moreover, to this day, standardization of an optimal sampling specimen for accurate cfDNA detection remains unclear with a choice between plasma and serum.

4. Exosome isolation techniques

4.1 Exosomes as a circulating biomarker

Exosomes are small membrane vesicles, 30–100 nm in size, released by cells into the extracellular space *via* the exocytosis pathway,[96,97] with composition and function dependent on the originating cell type.[98,99] Exosomes have specific surface markers on the plasma membrane and carry important gene regulatory content including proteins, microRNAs (miRs), and messenger RNAs (mRNAs).[100–103] It has been shown that exosomes act as vehicles for molecular cargo in cell–cell communication.[104–106] They can bind to the target cells through receptor–ligand interaction and participate in signaling events while circulating in the extracellular space.[107] They can also fuse with recipient-cell membranes to transport lipids, proteins, nucleic acids and ultimately be internalized by cells through endocytosis.[108] Studies have shown traces of exosomes in all human body fluids, including plasma, urine, saliva, tears, breast milk, and cerebral spinal fluid (CSF).[109,110] Exosomes can be found in large quantities in various tumor microenvironments,[111,112] which indicates their association with various cancers.[113–117] In cancer, exosomes have multifunctional roles including transferring oncogenes to target cells, promoting metastasis, facilitating immune system evasion, and stimulating angiogenesis and tumor growth.[118–120] Given these remarkable attributes, exosomes have a promising potential as biomarkers for cancer diagnostics and new semi-synthetic drug delivery vehicles for personalized therapy.[121–123]

4.2 Conventional methods for exosome isolation

Currently, differential ultracentrifugation is the gold standard for the purification and isolation of exosomes based on size. However, this technique is laborious, time-consuming, costly, and it requires large starting sample volumes. Isolation efficiency of exosomes by this method has a low recovery rate ranging from 5% to 25% and results in low purity.[124,125] To improve the yield and purity, density gradient separation has been added to the centrifugation steps.[126,127] However, the addition of an extra step to an already tedious isolation protocol results in more complication, time and cost. After the sample is purified, exosomes can be characterized by their hydrodynamic size[128] and protein contents.[129] Transmission Electron Microscopy (TEM) is a valuable imaging tool for measuring exosome sizes and visualizing shapes at single-molecule resolutions.[130] However, the throughput of the TEM technique is very low; and to incorporate high-throughput size distribution of exosomes the Nanoparticle Tracking Analysis (NTA) technology can be used. NTA relates the hydrodynamic radius of small particles to their Brownian motion, which is calculated by the Stokes–Einstein equation.[131] Afterwards, western blots can be used to analyze exosomal protein contents. Although these conventional methods are effective for initial exosome studies, their laborious and time-consuming nature imposes some inconsistencies in the downstream proteomic and genomic analyses.[132] Thus, in recent years, there has been a tremendous effort to develop microfluidic devices for high-throughput exosome isolation, detection and characterization.[15] Existing micro-/nano-scale devices can be classified into two major categories: size-based and immunoaffinity-based, which have been discussed in the following sections.

4.3 Size-based isolation

The size-based technologies can be divided into two modes: a passive and an active mode. In the passive mode, sorting depends on the inherent properties of exosomes or on the geometry of microfluidic channels, whereas the active separation mode relies on the interaction of exosomes with an external force. Devices designed utilizing these modes have been discussed below.

4.3.1 Passive isolation. Filtration is a widely used passive exosome isolation strategy. In a study by Wang *et al.* a microfluidic device with multidimensional hierarchical structure of silicon ciliated micropillars was developed to trap microvesicles (MVs) within the range of 30 to 200 nm in diameter.[133] In this device, silicon nano-wires were electrolessly etched on the micropillar sidewalls with the help of electrodeposited silver nanoparticle catalysts and porous microstructures were formed to trap the particles. The sample solution containing liposomes ~80 nm in diameter were flown through the micropillar region, which resulted in nearly 60% retention from a 30 μL sample. Further, trapped liposomes were easily released by saturating the porous silicon nanowire into the PBS solution for 24 hours, which led to nanowire degradation and thus, loosening the trapping sites.

The deterministic lateral displacement (DLD)-based microfluidic technique is another clever and promising passive method for the isolation of exosomes. In this technique the lateral shifts in each row of specifically arranged posts create individual streamlines which facilitate the nanoparticle separation. The geometry of the embedded gradient pillar arrays determines the cutoff diameter (D_c) of the particles and thus, particles smaller than D_c travel through the streamlines while the larger ones get laterally displaced.[61] For the first time, Santana *et al.* developed a DLD-based microfluidic obstacle array to separate cancer cell-derived microvesicles from heterogeneous extracellular shed vesicle populations with a cutoff threshold of 250 nm diameter.[134] The device prototype showed sorting of 190 nm fluorescent beads from 2 μm beads with a recovery efficiency of ~39% and purity of ~98.5% by volume. A validation experiment was conducted with extracellular shed vesicles (ESVs) extracted from the pancreatic adenocarcinoma BxPC-3 cell line. To authenticate the isolation results, vascular

endothelial growth factor (VEGF) was selected as the exemplary chemical readout, in which higher content of VEGF was observed on the captured MVs. The low recovery rate of the DLD-based isolation method was caused by the dominant role of small particle diffusion. Further research was done by Wunsch *et al.* involving fabricated pillar arrays with unique gap size ranging from 25 to 235 nm to separate colloids and exosomes.[135] They had demonstrated that at a low Péclet number, the particles between 20 and 100 nm were separated using the nano-DLD array. Also, exosomes within the size distribution of 60–70 nm from human urine were successfully isolated with this method.

Another innovative passive isolation strategy was based on the viscoelastic flow in microfluidic channels. The device relies on the size-dependent elastic lift forces exerted on the particles suspended in a viscoelastic medium to manipulate their motion.[136] Liu *et al.* have reported a platform to separate exosomes from cell culture media.[137] A biocompatible polymer poly-(oxyethylene) (PEO) was added as an additive into the medium to generate the lift force on the suspended EVs and control their lateral positions. The chip consisted of two inlets and three outlets, where the inlets introduced the sample and sheath fluids containing the PEO. Due to the small size of exosomes, they experienced less elastic force and remained at the wall while the large EVs were lifted in the center of the channel. The NTA measurement depicted high exosomal recovery of ~80% with a purity of ~90%.

Although, the passive microfluidic devices are label-free and independent of the external forces, they usually require dedicated fabrication procedures and equipment. Moreover, the sample processing time limits their high throughput, which challenges their use in clinical settings.

4.3.2 Active isolation. Active microfluidic devices incorporate external forces such as pressure, electric, or acoustic fields for size-based exosomal isolation. Although, the applied field makes the systems more complex, the magnitude of the forces can be controlled to achieve better efficiency and selectivity.

4.3.2.1 Pressure/electrokinetic filtration. Pressure driven microfluidic devices integrated with filter membranes have been reported for the purification of small EVs. For instance, Davies *et al.* used an innovative microfluidic filtration system in which nanoporous polymer membranes were integrated into poly(methyl methacrylate) (PMMA) chips by photopolymerization.[138] Small EVs from mouse blood were excluded through the nanoporous membrane under the applied pressure while cells and large debris remained. Although, the approach was highly size selective, the device was clogged after just 4 μL of sample filtration. To eliminate the clogging and improve the isolation purity, electrophoresis was performed to drive the negatively charged EVs across the membrane while the positively charged proteins were moved to the opposite direction. Similarly, Cho *et al.* employed the commercially available 30 nm polycarbonate porous membranes for the isolation of EVs from diluted plasma where the protein molecules with relatively smaller sizes were electrophoretically migrated through the membrane, whereas the larger EVs remained on the membrane surface.[139] This method presented a high recovery rate of 65%, which was estimated based on the RNA level and high purity of protein removal at 83.6% in 30 minutes. One major drawback of the electrophoresis-based approach has been the gas bubble formation at the electrodes, which hindered the flow through the channel when the applied electric field was larger than approximately 7 volts cm^{-1}. Another interesting electrophoresis independent isolation chip that used a pressure gradient to purify EVs was reported by Liu *et al.*[140] The samples were flushed through a parallel arrangement of nanoporous membranes with diameters in the range of 30 to 200 nm under the pressure generated by means of a syringe pump. This modular platform was capable of sorting the heterogeneous cancer-driven exosomes from a 10 mL sample in 3 hours. The EV isolation yield was estimated to be approximately 4 to 1000-fold higher than the traditional ultracentrifugation method.

4.3.2.2 Acoustic filtration. The acoustics-based isolation technique is a robust, label- and contact-free strategy that utilizes ultrasound waves to exert a radiation force on the particles in order to manipulate their motion. The force applied on the particles varies according to their mechanical properties such as size, density and compressibility.[141,142] Lee *et al.* reported an acoustic nano-filtration system (Fig. 5) that continuously filtered 10 μL of the packed red blood cell (pRBC) sample to separate exosomes from other biological contents.[143] Interdigitated transducer (IDT) electrodes fabricated on two ends of the device were used to generate a standing surface acoustic wave (SSAW) crossing the flow direction. An analytical model was constructed to fine-tune the cutoff size and obtain a binary separation. Thus, particles larger than

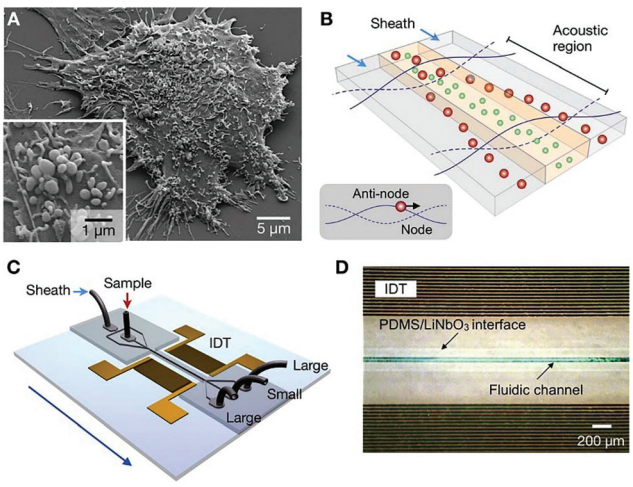

Fig. 5 The acoustic nanofilter for the separation of microvesicles.[143] (a) SEM image of MVs released by brain tumor cells (<1 μm in size). (b) The filter operation based on acoustic radiation pressure which transports MVs relatively based on their sizes. (c) The device schematic with a pair of interdigitated transducer (IDT) electrodes at its core and sample loading inlets and outlets. (d) The micrographs obtained from a prototype device showing IDT electrodes patterned on a piezoelectric substrate and the fluidic channel permanently bonded to the substrate.

the cutoff size in an acoustic field experienced higher radiation force and migrated towards the acoustic pressure nodes, whereas smaller particles were retained in the center. This device attained high isolation efficiency of ~80% recovery rate for exosomes suspended in the cell culture media.

4.3.2.3 Field flow fractionation. Flow field-flow fractionation (FFF) is an elution technique which is capable of separating nano-size molecules by differential retention in a liquid stream flowing through a channel.[144] In this regard, Moon's group proposed a miniaturized asymmetrical flow field-flow fractionation (AFlFFF) to separate exosomes based on their unique hydrodynamic diameters.[145,146] The electrical force was applied in perpendicular direction to the flow and thus particles suspended in the solution had varying retention ratios based on their sizes as the parabolic flow profile was applied in the channel. Thus, the smaller particles diffused further from the accumulation wall and were removed earlier from the channel compared to the larger ones. Exosomes were successfully fractionated from human neural stem cells at 1–2 minutes intervals and subsequently evaluated by transmission electron microscopy (TEM) and liquid chromatography-mass spectrometry. Furthermore, the same group used this approach to differentiate exosomes of prostate cancer (PCa) patients from healthy controls.[147] The quantitative lipidomic analysis was conducted on the collected exosomes *via* nano-flow ultrahigh performance liquid chromatography-electrospray ionization-tandem mass spectrometry (nUPLC-ESI-MS/MS) and selected reaction monitoring (SRM) methods to quantify the amount of lipids. Another group had optimized size-based FFF exosome isolation by incorporating in-line ultraviolet, dynamic light scattering (DLS) and multi-angle light scattering (MALS) detection for further characterization.[148]

4.3.2.4 Dielectrophoresis-based isolation. The dielectrophoresis-based method holds promising specifications for the isolation of target molecules including controllable manipulation, limited destructive impact on the sample and minimal sample pretreatment and collection procedures. Heller's group developed an alternating current electrokinetic (ACE) microarray chip device to isolate glioblastoma exosomes from the plasma sample.[149] The ACE chip consisted of a silicon base layer, platinum electrodes and a silicon dioxide layer; the edge of the silicon dioxide layer and the electrodes formed the dielectrophoretic high-field region which attracted only the nano-scaled molecules and excluded cells and larger entities. To prevent direct contact between the electrodes and the sample, a porous hydrogel layer was coated on the surface. A 30–50 μL plasma sample was used to isolate the glioblastoma exosomes by applying an AC voltage of 10 Vpp at 15 kHz. The residues were washed from the chip using the TE buffer and the trapped exosomes were released by reversing the direction of the dielectrophoretic force. Subsequently, on-chip fluorescence analysis using RNA Select Dye, fluorescently tagged anti-CD63 and anti-TSG101 antibodies was utilized to quantify the isolated exosomes. The entire on-chip exosomal isolation and quantification was completed within 30 minutes. They further applied this platform to isolate exosomes from serum and plasma from Pancreatic Ductal Adenocarcinoma (PDAC) patients with 99% sensitivity and 82% specificity.[150]

Although the active isolation schemes are relatively fast and label-free, due to the heterogeneity of the microvesicles and their size distribution variation, these isolation strategies cannot be utilized as the universal separation method for the isolation of exosomes with different biogenesis. Besides, the purity of collected exosomes based on their size has been unsatisfactory since contaminants such as protein aggregates, RNA–protein complexes and lipoproteins are in a similar size range.

4.4 Immunoaffinity-based approach

The first immunoaffinity-based exosomal isolation was reported by Chen *et al.*, in which a handheld microfluidic device was designed to capture exosomes with their unique membrane proteins from serum and cell culture media.[151] A herringbone engraved channel was designed in the device to enhance the mixing of samples with the immobilized antibodies (anti-CD63) on the channel surface. Exosomes were rapidly captured from 100 to 400 μL of serum in one hour and were further characterized by quantification of their RNA profiles using the RT-PCR technique. The recovery of EVs was in the range of 42–94% based on the amount of RNA that was extracted. Based on the same principle, Kanwar *et al.* fabricated a microfluidic device (Exo-chip) in a PDMS substrate and functionalized its surface with CD63 antibodies to capture and quantify exosomes from serum from pancreatic cancer patients.[152] The Exo-chip featured a planar structure of several circular wells connected by narrow channels to facilitate mixing and the use of a fluorescent carbocyanine dye (DiO) to specifically label exosomes for quantification. Abundant total protein yield of 15–18 μg and 10–15 ng nucleic acids were extracted from the exosomes that were isolated from 400 μL of serum.

In another attempt, a highly sensitive microfluidic platform with 3D structure had been developed by Zhang *et al.* for the immunological capture of exosomes and quantification of their marker expression levels *via* Enzyme Linked Immunosorbent Assay (ELISA).[153] The device featured an array of Y-shaped micro-posts with a coating of graphene oxide (GO) and polydopamine (PDA) on the surface. The GO/PDA interface created a 3D porous structure, which provided a larger surface area for high density antibody immobilization on the reactive sites. The Y-shaped micro-posts also improved the capture efficiency by bifurcating the flow and enhancing the mixing efficiency. Exosomes from the plasma sample of patients with ovarian cancer were isolated and quantified. The overall expression levels of both generic exosomal markers (CD9 and CD81) and the tumor-associated EpCAM marker were analyzed and presented as a united fluorescent signal, to increase the overall detection sensitivity. Results showed an increased expression level of the exosomal markers in ovarian cancer patients as compared to healthy controls.[153]

Besides relying only on microfluidics channel geometry for the immunoaffinity isolation of exosomes, spherical particles or immunomagnetic beads have been widely used to enhance their isolation efficiency. For instance, Dudani *et al.* used a flow cytometry setup interfacing with rapid inertial solution exchange (RInSE) to collect the exosomes by means of specific anti-CD63-polystyrene beads utilizing the inertial lift forces.[154] The exosome–particle complex was lifted in the center of a high aspect ratio microchannel and was isolated at the outlet while the smaller sized debris experienced a lower lifting force and thus was excluded from the side outlets. The experiments were conducted using blood samples from cultured melanoma cells and breast cancer cells with a throughput of 70 μL min^{-1}. The RNA content and the nucleotide length range extracted from the captured exosomes were quantified to validate the exosomal isolation success.

Furthermore, Rho *et al.* reported a micronuclear magnetic resonance (μNMR) system which was incorporated into a microfluidics platform (Fig. 6) to isolate and detect MVs in packed red blood cell (pRBC) units.[155] The MVs from 100 μL of pRBC sample were captured by antibody-coated polymer microbeads and collected *via* a membrane filter-assisted microfluidic device. Further, the collected MVs were labeled with CD235-specific magnetic nanoparticles and were detected using a miniaturized relaxometer developed by Issadore's group.[156] The μNMR measurements were carried out toward quantification of the isolated MVs with the entire process requiring only 30 minutes to complete.

A dual-purpose microfluidic chip containing a cascade of microchannel circuits for exosome isolation and immunoprecipitation has been reported by Godwin's group.[157] The objective of this integrated device was to conduct *in situ* exosomal protein analysis by means of a chemifluorescence-assisted sandwich immunoassay after the exosome isolation step. The chip was composed of an immunomagnetic isolation chamber where exosomes were captured onto antibody coated magnetic beads. Further, the captured exosomes were chemically lysed and the exosomal proteins were passed on to the next cascading stage. The proteins were captured with antibody-labeled magnetic beads, downstream in the design and lastly, chemifluorescence reagents were added for sandwich immunodetection of the circulating protein markers. Clinical application of this approach was proven with 30 μL plasma specimens from non-small-cell lung cancer (NSCLC) patients under 100 minutes while being able to profile the phenotypes associated with cancer. The system was robust with great bead capture efficiency of 99% observed over a variety of flow conditions. This study established a minimally invasive liquid biopsy technique using exosomes as circulating biomarkers as a great alternative to conventional invasive tissue biopsy. Later,

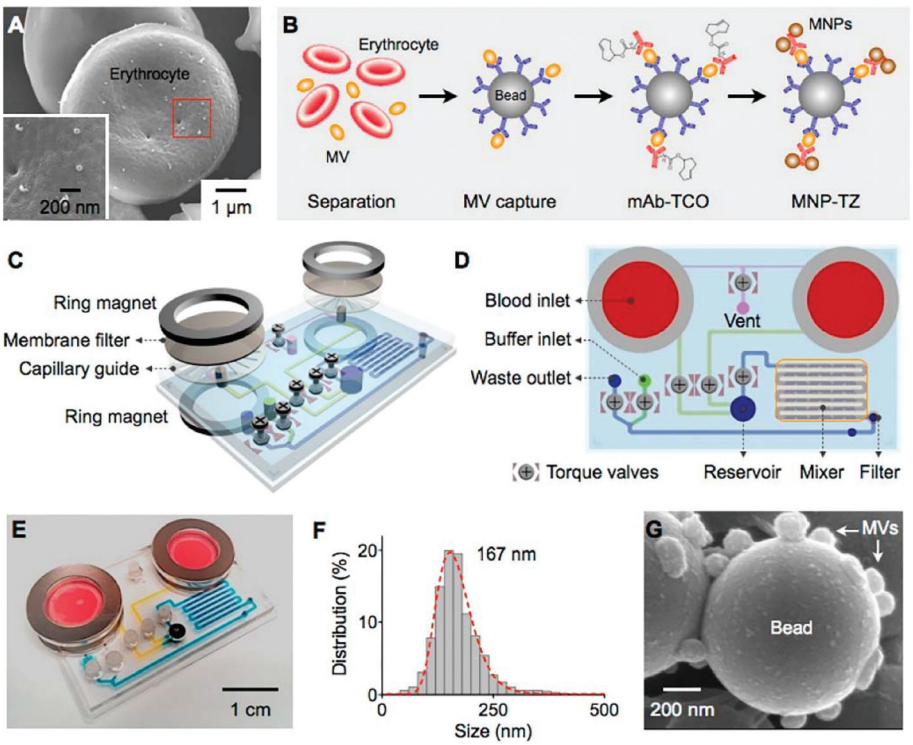

Fig. 6 The micronuclear magnetic resonance-based platform for microvesicle detection.[155] (a) A SEM image of an erythrocyte with microvesicles on the surface (microvesicles; inset) from an RBC cell. (b) The assay scheme design with Ab-coated microbeads. (c) The μNMR system depicting the membrane filter and capillary guide sandwiched between two ring magnets. (d) The device top-view with the different microfluidic components. (e) An actual picture of a prototype device. (f) The size distribution of filtered MVs analyzed by nanoparticle tracking analysis (NTA). (g) Electron microscopic image of the capture of microvesicles by microbeads.

the group improved the device by incorporating an on-chip exosome capture procedure, called ExoSearch.[158] They combined a Y-shaped injector and a serpentine fluidic mixer with the objective of enhancing the mixing efficiency of the immunomagnetic beads with plasma samples from the ovarian cancer patients. Rapid multiplex detection of three exosomal tumor markers (CA-125, EpCAM, and CD24) was achieved within 40 minutes using a small sample volume of 20 μL.

Another innovative exosomal isolation method by Ueda *et al.* established an antibody-coupled monolithic silica microtip array for exosome purification integrated with Mass Spectrometric Immunoassay (MSIA) for quantification.[159] Anti-CD9 antibodies were immobilized onto the porous monolithic silica microtips to specifically capture the tetraspanin molecule CD9 on the exosome membrane. These microtips, used in a multi-channel arrangement, provided a fast and reproducible exosome extraction mechanism and made the mass spectroscopic profiling process fairly streamlined. An automated 12-channel pipette system enabled simultaneous isolation of exosomes from 12 samples within 30 minutes and subsequently the isolated exosomal proteins were quantified by mass spectrometry. The results proved CD91 to be a specific exosomal marker in lung cancer.

Although the immunoaffinity based schemes for exosome purification are highly selective compared to the other techniques, still the nonspecific adsorption of other membrane vesicles has hindered the purity and efficiency outcome in some cases. This problem was addressed with an efficient vesicle extraction approach from a complex biological sample by Vaidyanathan *et al.* Their group developed an immunoaffinity-based microfluidic device with a tunable alternating current electrohydrodynamic (ac-EHD) method. The shear force induced by ac-EHD generated a nanoscale lateral fluidic flow at the electrode surface, which increased collision between the exosomes and antibodies and enhanced the exosomal capture efficiency while reducing the nonspecific binding.[160] Exosomes from breast cancer and prostate cancer cell lines were flown through the microfluidic device and captured by the immobilized antibodies on two asymmetric gold microelectrodes. Post capture, the introduction of horseradish peroxidase (HRP) antibody resulted in the catalytic oxidation of peroxidase and led to a visible colorimetric readout. Moreover, quantitative detection of the isolated exosomes was achieved with UV-visible spectroscopy measurements. Results showed the expression of human epidermal growth factor receptor 2 (HER2) and prostate specific antigen (PSA) in exosomes derived from breast cancer and prostatic cancer patients, respectively.

The immunological separation methods have high specificity for capturing pure EVs, but the recovery rate is poor due to the versatile classes of surface proteins found on different EVs. Further, the EVs are typically captured generically regardless of their cancerous relevance. Hence, microfluidics-based isolation of cancer-related EVs with good viability and purity remains a challenge when relying on generic markers or size-based approaches.

4.4.1 Surface plasma resonance (SPR)-based isolation and detection approach. Surface plasma resonance (SPR)-based nanosensors are widely used for the detection and characterization of small molecules. Im *et al.* developed a highly sensitive Surface Plasma Resonance (SPR)-based assay utilizing periodic nanoholes at the core of the sensing scheme, called the nanoplasmonic exosome (nPELX) assay for the detection of exosomes.[161] The device was composed of a 44 × 32 lattice of nanoholes, each with a diameter of 200 nm and a periodicity of 450 nm over a 200 nm-thick gold film. Antibodies against EpCAM, CD24 and CD63 were immobilized on the array, enabling the binding of ovarian cancer driven exosomal surface markers. A compact collinear optical setup and a sensing unit were constructed to measure the wavelength shifts in the light spectrum and intensity change upon exosomal binding to the nPLEX sensor. Results profiled the exosomal protein levels of EpCAM and CD24 expressed in ovarian cancer with an accuracy of 97%. A similar SPR-based sensor was developed by Zhu *et al.*, which utilized surface plasmon resonance imaging (SPRi) in combination with antibody microarrays against exosomal transmembrane proteins including tetraspanins, glycoproteins and tyrosine kinase receptors to isolate and quantify exosomes in the tumor cell culture medium.[162] Their device used a multiplex immunoaffinity approach to successfully capture exosomes from the cell culture supernatant without prior enrichment or purification. In addition, a charge-coupled device (CCD) camera was used to record the refractive index change caused by exosomal binding, achieving real-time exosomal detection.

Based on a similar mechanism, Rupert *et al.* explored the use of an SPR readout to determine the concentration of exosomes secreted from human mast cells.[163] The SPR surface was functionalized with anti-CD63 antibodies to measure the diffusion-limited binding rate of the exosomes. The SPR response was translated into a surface-bound mass. Over time, the increase in mass uptake was regarded a direct correlation to the exosomal content in the solution. This was further expressed mathematically, realizing the binding rate performed with controlled-flow conditions. This detection method presented great sensitivity with high signal-to-noise ratio (~100) at a detection limit in the picomolar range.

For a better understanding of the clinical significance of exosomes as cancer biomarkers, Sina *et al.* achieved specific isolation and quantification of clinically relevant exosomes (CREs) from the serum of breast cancer patient samples utilizing an SPR platform.[164] The initial isolation of exosomes was performed by utilizing the generic tetraspanin biomarkers (*i.e.*, CD9, CD63) and followed by specific detection of exosomal tumor-specific markers (*e.g.*, HER2). The results showed high platform sensitivity, being able to detect HER2 exosomes from samples containing roughly 2070 exosomes per μL. Approximately 14 to 34% of identified CREs out of the bulk exosome population expressed tumor-specific HER2 markers.

4.4.2 Flow cytometry-based isolation and detection. Flow cytometry is another powerful technique for EV detection in which vesicles tagged with a fluorescent label are hydrodyna-

mically focused in the fluid stream and detected by a laser beam with forward-scattered light (FSC) and side-scattered light (SSC).[165] Utilizing the Mie theory,[166] Van der Pol *et al.* correlated the amount of light scattered by a vesicle or a microparticle to its diameter while being able to detect a single large vesicle and a swarm of small vesicles.[167] The size of single vesicles with diameters in the range of 300–700 nm was estimated by means of flow cytometry, while multiple smaller vesicles were counted as a single event signal. Cell-derived vesicles from human urine in varying size distributions were also detected with this method. In another study, Van der Vlist *et al.* reported a detailed protocol on the flow cytometry detection of nano-sized vesicles, which used a commercial BD Influx Flow Cytometer to quantitatively and qualitatively analyze individual cell-derived vesicles ~100 nm in size.[168] An optimized fluorescent labelling protocol illustrated the capability of the BD Influx Cytometer to distinguish particles between 100 to 200 nm, based on their differences in the light scatter profiles. However, the conventional forward and side scatter based cytometer devices were limited in their operable scatter range (0.5–15°) due to their lower limit of detection and had failed in detecting the majority of EVs. A protocol aimed at resolving this issue had been reported by Pospichalova *et al.* to purify, quantify and characterize EVs from a cell culture medium using protein- and lipid-specific fluorescent dyes in approximately 12 hours.[169] In this method, a set of flow cytometry approaches were utilized knowing that the objects with sizes close to the observing wavelength (*e.g.* exosomes) scatter substantially more light at larger angles (15–150°) upon diffraction. Three different dedicated light scatter cytometry implementations including SALS (small angle light scatter), MALS (medium angle light scatter) and LALS (large angle light scatter) were deployed to estimate objects beyond the lower detection limit of FSC. Contrary to conventional cytometry, where unbound fluorescent dye has to be removed with an ultracentrifugation step, this method made that obsolete. Morales-Kastresana *et al.* studied a robust labeling method in a high-resolution flow cytometry approach by comparing three staining strategies: lipid-binding, protein-binding and nucleic acid-binding at a single EV resolution.[170] This nanoscale flow cytometry (NanoFACS) method used a more comprehensive technique by analyzing the dendritic cell samples (DC 2.4 cell line) with the combination of light scattering and fluorescence in cytometry while achieving successful resolution having removed the background noise. NanoFACS detection results with fluorescence intensities showed consistency when protein-binding dye 5-(and 6)-Carboxyfluorescein Diacetate Succinimidyl Ester (CFSE) was used as a label. Furthermore, size exclusion chromatography was utilized to remove the unbound labels, which preserved the biological function of EVs regarding their structural or functional integrity.

Despite the utility of flow cytometry as the vesicle isolation technique, it has its own challenges at the nanoscale. The extremely small size of EVs makes their surface markers difficult to label and as a result using flow cytometry for quantifying them became a tedious task. To address this limitation, Löf *et al.* utilized the magnetic bead-based assay combined with a multicolor *in situ* proximity ligation assay (PLA), which labelled EVs in three distinguishable colors to amplify the signal of individual EVs.[171] Oligonucleotide conjugated capturing antibodies (anti-CD63) were first immobilized on the surface of streptavidin-modified magnetic beads. After capturing the EVs on the beads, four PLA probes containing antibodies against CD26, CD10, CD13 and cathepsin B were added into the solution to bind with EVs. This step led to DNA circularization *via* enzymatic ligation. Next, enzymatic digestion released EVs from the beads and was followed by rolling circle amplification[172] which amplified the three differently colored signals. This method produced sufficient fluorophores at each EV enabling easy detection with flow cytometry.

Although, flow cytometry is a powerful method to qualitatively and quantitatively detect cells, it has its limitations for extracellular vesicle characterization due to their small size, heterogeneity and their low refractive index. The individual small EVs are difficult to be distinguished from their background with traditional flow cytometry, which has a size detection threshold of ~500 nm (ref. 173) and often background noise hinders the analysis. In addition, small EVs have a limited number of antigens on their membrane to be labelled which makes scatter-based detection an uphill task.

Research aimed at the isolation of EVs based on microfluidic techniques is still in the early stages of development. Among the emerging isolation techniques, most methods have been based on either size differences or exosomal specific markers. In the time to come, advances towards EV detection and separation based on their biophysical properties could be highly promising. An overview of EV isolation and detection techniques has been provided in Tables 2 and 3.

5. Summary

Cancer diagnostics and prognostics are currently obtained by either the standard tissue biopsy approach or by expensive and bulky imaging techniques. Consequently, liquid biopsy has recently gained attention as a minimally invasive approach to provide a more holistic snapshot of the cancerous aberrations. The migration of isolation techniques towards a microfluidics centered design has been on the rise. These miniaturized devices focusing on liquid biopsy, utilizing a patient's blood, urine, plasma or serum sample, have been developed to understand genomic and proteomic evolution, associated with primary and metastatic spread of cancer. The use of microfluidic devices requires much smaller sample volumes for analysis and less or no-sample preparation in most designs. Also, the rapid processing of results with high specificity and enhanced levels of sensitivity has lured researchers to utilise their potential to the maximum.

Tumor derived exosomes, circulating tumor cells in the bloodstream or short-living cfDNA, all have provided a great deal of information proving their clinical relevance in carcinoma detection and monitoring. However, studies have

Table 2 Summary of EV isolation techniques

Platform	Separation method	Sample	Volume	Isolation time	Recovery rate	Advantages	Ref.
Size-based passive isolation	Sieving	Liposomes	30 μL	10 min	60%	Label-free, rapid	133
	DLD-based	Cell culture supernatant	200 μL	—	—	Label-free, easy to operate	134
		Commercial urine-derived exosomes	0.72 μL	—			135
	Viscoelasticity-based	Cell culture medium	100 μL	—	93.6%	Label-free, simple	137
Size-based active isolation	Pressure/electrokinetic filtration on porous structure	Mouse blood	240 μL	—	—	Label-free	138
		Mouse plasma	500 μL		65%		139
		Cell culture media	—	—	—		140
	Acoustic filtration	Packed RBC units	10 μL	—	80%	Label-free, rapid	143
	Field flow fractionation-based isolation	Human neural stem cells	1–2 mL	—	—	High specificity	145 and 146
	Dielectrophoresis-based isolation	Plasma, serum	30–50 μL	<30 min		Rapid, label-free	149 and 150
Immunoaffinity-based isolation	Antibody antigen specific binding	Serum	400 μL	<1 hour	42–94%	High specificity, high efficiency	148
		Serum	400 μL	50 min	-—		152
		Serum	350 μL	30 min	—		159
	Nano-shearing	Cell culture supernatant and serum	500 μL	—	—		160
	Nano-IMEX	Plasma	20 μL	—	—		153
	Inertial solution exchange	Blood	—	—	—		154
	Micronuclear magnetic resonance (μNMR)-based	Blood	100 μL	—	—		155
	Magnetic beads-based	Human plasma	30 μL	1.5 hours	—		157
		Plasma	20 μL	40 min	72%		158

Table 3 Summary of EV optical detection techniques

Detection approach	Sample	Advantage	Ref.
Surface plasma resonance (SPR)-based	Ascites	Sensitive, high throughput, real time detection, label-free	161
	Cell culture supernatant		162
	Cell culture supernatant		163
	Serum		164
Flow cytometry-based	Human urine	High-throughput, accurate	167
	Cell culture supernatant		168
	Cell culture supernatant		169
	Cell culture supernatant		170
	Cell culture supernatant		171

depicted that there are different challenges with each biomarker that limit its current detection capability or isolation efficiency. Several types of tumor progressions do not necessarily release substantial CTCs in the bloodstream, if at all.[174] This poses challenges at the small sample volume levels to conduct any analysis. With filtration, clogging has been an issue and a precise control on the cut-off threshold for cell size has been difficult. Immunoaffinity oriented designs are limited by inconsistencies in expression levels leading to low capture rates. More work on the morphological as well as molecular characterization of CTCs would lead to a better comprehension of the biology of metastasis in cancer patients and eventually help with their prognosis. cfDNA, on the contrary, are abundant in the human system. However, low recovery yield, poor target specificity and the absence of a standard sampling specimen (between plasma and serum) remains an unanswered question. The major issue with sensing exosomes is their differentiation from other microvesicles shed from cells. Similar size and density or scatter properties of any vesicle would make the detection and isolation of the target exosomes challenging. Meanwhile, the purity and the recovery rate have been questionable with the microfluidic approaches employed in their extraction. Besides, current studies on exosome analysis are conducted *in vitro* and very little is known about their physiological behavior in an *in vivo* setting.

The need of the hour is to develop technologies that can meet these requirements and isolate the biomarkers from a mixture of various elements and impurities. For a better clinical utility, besides being able to carry out detection and isolation, the same microfluidic device should perform the downstream analysis on the contents of segregated tumor cells or microvesicles. The promising devices discussed in this review must be tested with a large cohort of patients before their clinical relevance can be established. Further, with the progression of cancer, the concentration of CTCs and exosomes in the patient's body fluid varies continuously and requires constant adjustments in treatment.[175] Therefore, isolation and

analysis of one biomarker by itself might be promising but not necessarily be a more reliable diagnostic approach. Strides must be made towards integrating the existing and upcoming approaches to provide a more optimized answer with improved accuracy in detection thereafter. An approach that caters to both genomic and proteomic aspects of analysis on the isolated biomarkers would be a lot more interrogative and real-time than the currently existing models. With quite a few integrative designs, operational mechanisms such as inertial isolation and magnetophoresis have already been employed together towards CTC isolation.[176] By combining their enrichment approaches with abundantly observed microvesicles, an improved genome status of carcinoma and data on its progression through different stages can be accurately studied. Such microfluidic assays would hold true and have more systematic clinical relevance and would make way for more reliable means towards the understanding of cancer.

Conflicts of interest

There are no conflicts of interest to declare.

References

1 J. Ferlay, I. Soerjomataram, R. Dikshit, S. Eser, C. Mathers, M. Rebelo, D. M. Parkin, D. Forman and F. Bray, *Int. J. Cancer*, 2015, **136**, E359–E386.
2 National Cancer Institute Online, https://www.cancer.gov/about-cancer/screening/screening-tests, (accessed March 2015).
3 B. Gold, M. Cankovic, L. V. Furtado, F. Meier and C. D. Gocke, *J. Mol. Diagn.*, 2015, **17**, 209–224.
4 E. Crowley, F. Di Nicolantonio, F. Loupakis and A. Bardelli, *Nat. Rev. Clin. Oncol.*, 2013, **10**, 472–484.
5 K.-A. Hyun, J. Kim, H. Gwak and H.-I. Jung, *Analyst*, 2016, **141**, 382–392.
6 S. A. Soper and A. Rasooly, *Analyst*, 2016, **141**, 367–370.
7 J. C. Contreras-Naranjo, H.-J. Wu and V. M. Ugaz, *Lab Chip*, 2017, **17**, 3558–3577.
8 A. Liga, A. Vliegenthart, W. Oosthuyzen, J. Dear and M. Kersaudy-Kerhoas, *Lab Chip*, 2015, **15**, 2388–2394.
9 H. Kang, J. Kim and J. Park, *Micro Nano Syst. Lett.*, 2017, **5**, 15.
10 M. T. Gabriel, L. R. Calleja, A. Chalopin, B. Ory and D. Heymann, *Clin. Chem.*, 2016, **62**, 571–581.
11 I. Cima, C. Wen Yee, F. S. Iliescu, W. Min Phyo, K. Hon Lim, C. Iliescu and M. Han Tan, *Biomicrofluidics*, 2013, **7**, 011810.
12 H. Esmaeilsabzali, T. V. Beischlag, M. E. Cox, A. M. Parameswaran and E. J. Park, *Biotechnol. Adv.*, 2013, **31**, 1063–1084.
13 K.-A. Hyun and H.-I. Jung, *Lab Chip*, 2014, **14**, 45–56.
14 M. Ignatiadis and M. Reinholz, *Breast Cancer Res.*, 2011, **13**, 222.
15 J. Ko, E. Carpenter and D. Issadore, *Analyst*, 2016, **141**, 450–460.
16 J. den Toonder, *Lab Chip*, 2011, **11**, 375–377.
17 G. Attard and J. S. de Bono, *Curr. Opin. Genet. Dev.*, 2011, **21**, 50–58.
18 M. G. Lee, J. H. Shin, C. Y. Bae, S. Choi and J.-K. Park, *Anal. Chem.*, 2013, **85**, 6213–6218.
19 M. Zborowski and J. J. Chalmers, *Anal. Chem.*, 2011, **83**, 8050–8056.
20 S. Maheswaran, L. V. Sequist, S. Nagrath, L. Ulkus, B. Brannigan, C. V. Collura, E. Inserra, S. Diederichs, A. J. Iafrate, D. W. Bell, S. Digumarthy, A. Muzikansky, D. Irimia, J. Settleman, R. G. Tompkins, T. J. Lynch, M. Toner and D. A. Haber, *N. Engl. J. Med.*, 2008, **359**, 366–377.
21 S. Seal, *Cancer*, 1964, **17**, 637–642.
22 P. R. Gascoyne, J. Noshari, T. J. Anderson and F. F. Becker, *Electrophoresis*, 2009, **30**, 1388–1398.
23 Y. Chen, P. Li, P.-H. Huang, Y. Xie, J. D. Mai, L. Wang, N.-T. Nguyen and T. J. Huang, *Lab Chip*, 2014, **14**, 626–645.
24 H. Mohamed, M. Murray, J. N. Turner and M. Caggana, *J. Chromatogr., A*, 2009, **1216**, 8289–8295.
25 M. Al-Hajj, M. S. Wicha, A. Benito-Hernandez, S. J. Morrison and M. F. Clarke, *Proc. Natl. Acad. Sci. U. S. A.*, 2003, **100**, 3983–3988.
26 D. Antolovic, L. Galindo, A. Carstens, N. Rahbari, M. W. Büchler, J. Weitz and M. Koch, *BMC Biotechnol.*, 2010, **10**, 35.
27 A. Truini, A. Alama, M. G. Dal Bello, S. Coco, I. Vanni, E. Rijavec, C. Genova, G. Barletta, F. Biello and F. Grossi, *Front. Oncol.*, 2014, **4**, 242.
28 I. Van der Auwera, D. Peeters, I. Benoy, H. Elst, S. Van Laere, A. Prove, H. Maes, P. Huget, P. Van Dam, P. Vermeulen and L. Y. Dirix, *Br. J. Cancer*, 2010, **102**, 276–284.
29 G. Vona, A. Sabile, M. Louha, V. Sitruk, S. Romana, K. Schütze, F. Capron, D. Franco, M. Pazzagli, M. Vekemans, B. Lacour, C. Bréchot and P. P. Bréchot, *Am. J. Pathol.*, 2000, **156**, 57–63.
30 S. Zheng, H. K. Lin, B. Lu, A. Williams, R. Datar, R. J. Cote and Y.-C. Tai, *Biomed. Microdevices*, 2011, **13**, 203–213.
31 S. J. Tan, L. Yobas, G. Y. H. Lee, C. N. Ong and C. T. Lim, *Biomed. Microdevices*, 2009, **11**, 883–892.
32 S. Zheng, H. Lin, J.-Q. Liu, M. Balic, R. Datar, R. J. Cote and Y.-C. Tai, *J. Chromatogr., A*, 2007, **1162**, 154–161.
33 T.-H. Kim, M. Lim, J. Park, J. M. Oh, H. Kim, H. Jeong, S. J. Lee, H. C. Park, S. Jung, B. C. Kim, K. Lee, M. Kim, D. Y. Park, G. H. Kim and Y. Cho, *Anal. Chem.*, 2016, **89**, 1155–1162.
34 X. Qin, S. Park, S. P. Duffy, K. Matthews, R. R. Ang, T. Todenhöfer, H. Abdi, A. Azad, J. Bazov, K. N. Chi, P. C. Chi and H. Ma, *Lab Chip*, 2015, **15**, 2278–2286.
35 A. F. Sarioglu, N. Aceto, N. Kojic, M. C. Donaldson, M. Zeinali, B. Hamza, A. Engstrom, H. Zhu, T. K. Sundaresan, D. T. Miyamoto, X. Luo, A. Bardia,

B. S. Wittner, S. Ramaswamy, T. Shioda, D. T. Ting, S. L. Stott, R. Kapur, S. Maheswaran, D. A. Haber and M. Toner, *Nat. Methods*, 2015, **12**, 685–691.
36 W.-P. Chou, H.-M. Wang, J.-H. Chang, T.-K. Chiu, C.-H. Hsieh, C.-J. Liao and M.-H. Wu, *Sens. Actuators, B*, 2017, **241**, 245–254.
37 H. Andersson and A. Van den Berg, *Sens. Actuators, B*, 2003, **92**, 315–325.
38 T. Sun and H. Morgan, *Microfluid. Nanofluid.*, 2010, **8**, 423–443.
39 K.-H. Han, A. Han and A. B. Frazier, *Biosens. Bioelectron.*, 2006, **21**, 1907–1914.
40 A. Han, L. Yang and A. B. Frazier, *Clin. Cancer Res.*, 2007, **13**, 139–143.
41 P. S. Hair, K. H. Schoenbach and E. S. Buescher, *Bioelectrochemistry*, 2003, **61**, 65–72.
42 H. Shafiee, M. B. Sano, E. A. Henslee, J. L. Caldwell and R. V. Davalos, *Lab Chip*, 2010, **10**, 438–445.
43 Y. Kang, D. Li, S. A. Kalams and J. E. Eid, *Biomed. Microdevices*, 2008, **10**, 243–249.
44 Y. Zhang, C.-W. Lo, J. A. Taylor and S. Yang, *Langmuir*, 2006, **22**, 8595–8601.
45 S. S. Kuntaegowdanahalli, A. A. S. Bhagat, G. Kumar and I. Papautsky, *Lab Chip*, 2009, **9**, 2973–2980.
46 N. Nivedita, N. Garg, A. P. Lee and I. Papautsky, *Analyst*, 2017, **142**, 2558–2569.
47 E. Sollier, D. E. Go, J. Che, D. R. Gossett, S. O'Byrne, W. M. Weaver, N. Kummer, M. Rettig, J. Goldman, N. Nickols, M. Rettig, J. Goldman, N. Nickols, S. McCloskey, R. P. Kulkarni and D. D. Carlo, *Lab Chip*, 2014, **14**, 63–77.
48 M. E. Warkiani, G. Guan, K. B. Luan, W. C. Lee, A. A. S. Bhagat, P. K. Chaudhuri, D. S.-W. Tan, W. T. Lim, S. C. Lee, P. C. Chen, C. T. Lim and J. Han, *Lab Chip*, 2014, **14**, 128–137.
49 E. S. Park, C. Jin, Q. Guo, R. R. Ang, S. P. Duffy, K. Matthews, A. Azad, H. Abdi, T. Todenhöfer, J. Bazov, K. N. Chi, P. C. Black and H. Ma, *Small*, 2016, **12**, 1909–1919.
50 H. Amini, W. Lee and D. Di Carlo, *Lab Chip*, 2014, **14**, 2739–2761.
51 A. A. Adams, P. I. Okagbare, J. Feng, M. L. Hupert, D. Patterson, J. Göttert, R. L. McCarley, D. Nikitopoulos, M. C. Murphy and S. A. Soper, *J. Am. Chem. Soc.*, 2008, **130**, 8633–8641.
52 R. R. Henriquez, T. Ito, L. Sun and R. M. Crooks, *Analyst*, 2004, **129**, 478–482.
53 S. Nagrath, L. V. Sequist, S. Maheswaran, D. W. Bell, D. Irimia, L. Ulkus, M. R. Smith, E. L. Kwak, S. Digumarthy, A. Muzikansky, P. Ryan, U. J. Balis, R. G. Tompkins, D. A. Haber and M. Toner, *Nature*, 2007, **450**, 1235–1239.
54 J. H. Kang, S. Krause, H. Tobin, A. Mammoto, M. Kanapathipillai and D. E. Ingber, *Lab Chip*, 2012, **12**, 2175–2181.
55 S. L. Stott, C.-H. Hsu, D. I. Tsukrov, M. Yu, D. T. Miyamoto, B. A. Waltman, S. M. Rothenberg, A. M. Shah, M. E. Smas, G. K. Korir, F. P. Floyd, A. J. Gilman, J. B. Lord, D. Winokur, S. Springer, D. Irimia, S. Nagrath, L. V. Sequist, R. J. Lee, K. J. Isselbacher, S. Maheswaran, D. A. Haber and M. Toner, *Proc. Natl. Acad. Sci. U. S. A.*, 2010, **107**, 18392–18397.
56 M.-H. Park, E. Reátegui, W. Li, S. N. Tessier, K. H. Wong, A. E. Jensen, V. Thapar, D. Ting, M. Toner, S. L. Stott and P. T. Hammond, *J. Am. Chem. Soc.*, 2017, **139**, 2741–2749.
57 M. Münz, A. Murr, M. Kvesic, D. Rau, S. Mangold, S. Pflanz, J. Lumsden, J. Volkland, J. Fagerberg, G. Riethmüller, D. Rüttinger, P. Kufer, P. A. Baeuerle and T. Raum, *Cancer Cell Int.*, 2010, **10**, 44.
58 T. M. Gorges, I. Tinhofer, M. Drosch, L. Röse, T. M. Zollner, T. Krahn and O. von Ahsen, *BMC Cancer*, 2012, **12**, 178.
59 N. M. Karabacak, P. S. Spuhler, F. Fachin, E. J. Lim, V. Pai, E. Ozkumur, J. M. Martel, N. Kojic, K. Smith, P.-i. Chen, J. Yang, H. Hwang, B. Morgan, J. Trautwein, T. A. Barber, S. L. Stott, S. Maheswaran, R. Kapur, D. A. Haber and M. Toner, *Nat. Protoc.*, 2014, **9**, 694–710.
60 M. Yu, A. Bardia, B. S. Wittner, S. L. Stott, M. E. Smas, D. T. Ting, S. J. Isakoff, J. C. Ciciliano, M. N. Wells, A. M. Shah, K. F. Concannon1, M. C. Donaldson1, L. V. Sequist, E. Brachtel, D. Sgroi, J. Baselga, S. Ramaswamy, M. Toner, D. A. Haber and S. Maheswaran, *Science*, 2013, **339**, 580–584.
61 L. R. Huang, E. C. Cox, R. H. Austin and J. C. Sturm, *Science*, 2004, **304**, 987–990.
62 D. Di Carlo, D. Irimia, R. G. Tompkins and M. Toner, *Proc. Natl. Acad. Sci. U. S. A.*, 2007, **104**, 18892–18897.
63 N. Pamme and A. Manz, *Anal. Chem.*, 2004, **76**, 7250–7256.
64 O. C. Farokhzad, S. Jon, A. Khademhosseini, T.-N. T. Tran, D. A. LaVan and R. Langer, *Cancer Res.*, 2004, **64**, 7668–7672.
65 K.-M. Song, S. Lee and C. Ban, *Sensors*, 2012, **12**, 612–631.
66 J. A. Phillips, Y. Xu, Z. Xia, Z. H. Fan and W. Tan, *Anal. Chem.*, 2008, **81**, 1033–1039.
67 D. Shangguan, Y. Li, Z. Tang, Z. C. Cao, H. W. Chen, P. Mallikaratchy, K. Sefah, C. J. Yang and W. Tan, *Proc. Natl. Acad. Sci. U. S. A.*, 2006, **103**, 11838–11843.
68 W. Sheng, T. Chen, R. Kamath, X. Xiong, W. Tan and Z. H. Fan, *Anal. Chem.*, 2012, **84**, 4199–4206.
69 D. Issadore, J. Chung, H. Shao, M. Liong, A. A. Ghazani, C. M. Castro, R. Weissleder and H. Lee, *Sci. Transl. Med.*, 2012, **4**, 141ra192.
70 M. Muluneh and D. Issadore, *Lab Chip*, 2014, **14**, 4552–4558.
71 B. Kwak, J. Lee, D. Lee, K. Lee, O. Kwon, S. Kang and Y. Kim, *Biosens. Bioelectron.*, 2017, **88**, 153–158.
72 L. Xiao, Z.-B. He, B. Cai, L. Rao, L. Cheng, W. Liu, S.-S. Guo and X.-Z. Zhao, *Chem. Phys. Lett.*, 2017, **668**, 35–41.
73 T. Y. Lee, K.-A. Hyun, S.-I. Kim and H.-I. Jung, *Sens. Actuators, B*, 2017, **238**, 1144–1150.

74 K. Kim, D. G. Shin, M. K. Park, S. H. Baik, T. H. Kim, S. Kim and S. Lee, *Ann. Surg. Treat. Res.*, 2014, **86**, 136–142.
75 H. Schwarzenbach, D. S. Hoon and K. Pantel, *Nat. Rev. Cancer*, 2011, **11**, 426–437.
76 L. A. Diaz Jr. and A. Bardelli, *J. Clin. Oncol.*, 2014, **32**, 579–586.
77 C. Hufnagl, M. Stöcher, M. Moik, R. Geisberger and R. Greil, *J. Nucleic Acids Invest.*, 2013, **4**, e1.
78 J. A. Shaw, K. Page, K. Blighe, N. Hava, D. Guttery, B. Ward, J. Brown, C. Ruangpratheep, J. Stebbing, R. Payne, C. Palmieri, S. Cleator, R. A. Walker and R. C. Coombes, *Genome Res.*, 2012, **22**, 220–231.
79 W. Yan, A. Zhang and M. J. Powell, *Chin. J. Cancer*, 2016, **35**, 68.
80 D. A. Haber and V. E. Velculescu, *Cancer Discovery*, 2014, **4**, 650–661.
81 S. Volik, M. Alcaide, R. D. Morin and C. Collins, *Mol. Cancer Res.*, 2016, **14**, 898–908.
82 H. Schwarzenbach, D. S. Hoon and K. Pantel, *Nat. Rev. Cancer*, 2011, **11**, 426–437.
83 K. Page, D. S. Guttery, N. Zahra, L. Primrose, S. R. Elshaw, J. H. Pringle, K. Blighe, S. D. Marchese, A. Hills, L. Woodley, J. Stebbing, R. C. Coombes and J. A. Shaw, *PLoS One*, 2013, **8**, e77963.
84 E. Heitzer, P. Ulz and J. B. Geigl, *Clin. Chem.*, 2015, **61**, 112–123.
85 F. M. Lun, R. W. Chiu, K. A. Chan, T. Y. Leung, T. K. Lau and Y. D. Lo, *Clin. Chem.*, 2008, **54**, 1664–1672.
86 A. Sonnenberg, J. Y. Marciniak, L. Rassenti, E. M. Ghia, E. A. Skowronski, S. Manouchehri, J. McCanna, G. F. Widhopf, T. J. Kipps and M. J. Heller, *Clin. Chem.*, 2014, **60**, 500–509.
87 A. Sonnenberg, J. Y. Marciniak, E. A. Skowronski, S. Manouchehri, L. Rassenti, E. M. Ghia, G. F. Widhopf, T. J. Kipps and M. J. Heller, *Electrophoresis*, 2014, **35**, 1828–1836.
88 A. Sonnenberg, J. Y. Marciniak, J. McCanna, R. Krishnan, L. Rassenti, T. J. Kipps and M. J. Heller, *Electrophoresis*, 2013, **34**, 1076–1084.
89 G. Sozzi, D. Conte, M. Leon, R. Cirincione, L. Roz, C. Ratcliffe, E. Roz, N. Cirenei, M. Bellomi, G. Pelosi, M. A. Pierotti and U. Pastorino, *J. Clin. Oncol.*, 2003, **21**, 3902–3908.
90 T.-L. Wu, D. Zhang, J.-H. Chia, K.-C. Tsao, C.-F. Sun and J. T. Wu, *Clin. Chim. Acta*, 2002, **321**, 77–87.
91 E. Gormally, E. Caboux, P. Vineis and P. Hainaut, *Mutat. Res., Rev. Mutat. Res.*, 2007, **635**, 105–117.
92 J. Jen, L. Wu and D. Sidransky, *Ann. N. Y. Acad. Sci.*, 2000, **906**, 8–12.
93 J. Yang, P. R. Selvaganapathy, T. J. Gould, D. J. Dwivedi, D. Liu, A. E. Fox-Robichaudc and P. C. Liaw, *Lab Chip*, 2015, **15**, 3925–3933.
94 D. Heineck, J. Lewis and M. Heller, *Electrophoresis*, 2017, **38**, 1475–1482.
95 S. Jeon, H. Lee, K. Bae, K.-A. Yoon, E. S. Lee and Y. Cho, *Theranostics*, 2016, **6**, 828–836.
96 H. Kalra, G. P. Drummen and S. Mathivanan, *Int. J. Mol. Sci.*, 2016, **17**, 170.
97 S. Keller, M. P. Sanderson, A. Stoeck and P. Altevogt, *Immunol. Lett.*, 2006, **107**, 102–108.
98 C. Théry, L. Zitvogel and S. Amigorena, *Nat. Rev. Immunol.*, 2002, **2**, 569–579.
99 A. V. Vlassov, S. Magdaleno, R. Setterquist and R. Conrad, *Biochim. Biophys. Acta, Gen. Subj.*, 2012, **1820**, 940–948.
100 R. M. Johnstone, *Blood Cells, Mol., Dis.*, 2006, **36**, 315–321.
101 H. Valadi, K. Ekström, A. Bossios, M. Sjöstrand, J. J. Lee and J. O. Lötvall, *Nat. Cell Biol.*, 2007, **9**, 654–659.
102 J. Zhang, S. Li, L. Li, M. Li, C. Guo, J. Yao and S. Mi, *Genomics, Proteomics Bioinf.*, 2015, **13**, 17–24.
103 A. van Hoof and R. Parker, *Cell*, 1999, **99**, 347–350.
104 M. Simons and G. Raposo, *Curr. Opin. Cell Biol.*, 2009, **21**, 575–581.
105 G. Camussi, M. C. Deregibus, S. Bruno, V. Cantaluppi and L. Biancone, *Kidney Int.*, 2010, **78**, 838–848.
106 M. Record, K. Carayon, M. Poirot and S. Silvente-Poirot, *Biochim. Biophys. Acta, Mol. Cell Biol. Lipids*, 2014, **1841**, 108–120.
107 R. Marhaba, P. Klingbeil, T. Nuebel, I. Nazarenko, M. W. Buechler and M. Zoeller, *Curr. Mol. Med.*, 2008, **8**, 784–804.
108 C. Corrado, S. Raimondo, A. Chiesi, F. Ciccia, G. De Leo and R. Alessandro, *Int. J. Mol. Sci.*, 2013, **14**, 5338–5366.
109 S. Keller, J. Ridinger, A.-K. Rupp, J. W. Janssen and P. Altevogt, *J. Transl. Med.*, 2011, **9**, 86.
110 J. Lin, J. Li, B. Huang, J. Liu, X. Chen, X.-M. Chen, Y.-M. Xu, L.-F. Huang and X.-Z. Wang, *Sci. World J.*, 2015, 657086.
111 F. Cappello, M. Logozzi, C. Campanella, C. C. Bavisotto, A. Marcilla, F. Properzi and S. Fais, *Eur. J. Pharm. Sci.*, 2017, **96**, 93–98.
112 R. Nedaeinia, M. Manian, M. Jazayeri, M. Ranjbar, R. Salehi, M. Sharifi, F. Mohaghegh, M. Goli, S. Jahednia, A. Avan and M. Ghayour-Mobarhan, *Cancer Gene Ther.*, 2017, **24**, 48–56.
113 D. D. Taylor and C. Gercel-Taylor, *Gynecol. Oncol.*, 2008, **110**, 13–21.
114 G. Rabinowits, C. Gerçel-Taylor, J. M. Day, D. D. Taylor and G. H. Kloecker, *Clin. Lung Cancer*, 2009, **10**, 42–46.
115 V. R. Minciacchi, M. R. Freeman and D. Di Vizio, *Semin. Cell Dev. Biol.*, 2015, **40**, 41–51.
116 J. Skog, T. Wurdinger, S. Van Rijn, D. Meijer, L. Gainche, M. Sena-Esteves, W. T. Curry Jr., R. S. Carter, A. M. Krichevsky and X. O. Breakefield, *Nat. Cell Biol.*, 2008, **10**, 1470–1476.
117 C. Wu, S. Du, J. Zhang, A. Liang and Y. Liu, *Cancer Gene Ther.*, 2017, **24**, 6–12.
118 C. Kahlert and R. Kalluri, *J. Mol. Med.*, 2013, **91**, 431–437.
119 A. S. Azmi, B. Bao and F. H. Sarkar, *Cancer Metastasis Rev.*, 2013, **32**, 623–642.
120 X. Zhang, X. Yuan, H. Shi, L. Wu, H. Qian and W. Xu, *J. Hematol. Oncol.*, 2015, **8**, 83.
121 P. Munson and A. Shukla, *Medicines*, 2015, **2**, 310–327.

122 R. S. Conlan, S. Pisano, M. I. Oliveira, M. Ferrari and I. M. Pinto, *Trends Mol. Med.*, 2017, **23**, 636–650.
123 J. Wang, Y. Zheng and M. Zhao, *Front. Pharmacol.*, 2017, **7**, 533.
124 H. G. Lamparski, A. Metha-Damani, J.-Y. Yao, S. Patel, D.-H. Hsu, C. Ruegg and J.-B. Le Pecq, *J. Immunol. Methods*, 2002, **270**, 211–226.
125 M. A. Livshits, E. Khomyakova, E. G. Evtushenko, V. N. Lazarev, N. A. Kulemin, S. E. Semina, E. V. Generozov and V. M. Govorun, *Sci. Rep.*, 2015, **5**, 17319.
126 R. Cantin, J. Diou, D. Bélanger, A. M. Tremblay and C. Gilbert, *J. Immunol. Methods*, 2008, **338**, 21–30.
127 D. W. Greening, R. Xu, H. Ji, B. J. Tauro and R. J. Simpson, *Proteomic Profiling: Methods and Protocols*, 2015, vol. 1295, pp. 179–209.
128 C. Y. Soo, Y. Song, Y. Zheng, E. C. Campbell, A. C. Riches, F. Gunn-Moore and S. J. Powis, *Immunology*, 2012, **136**, 192–197.
129 J. Schageman, E. Zeringer, M. Li, T. Barta, K. Lea, J. Gu, S. Magdaleno, R. Setterquist and A. V. Vlassov, *BioMed Res. Int.*, 2013, **2013**, 253957.
130 Y. Wu, W. Deng and D. J. Klinke II, *Analyst*, 2015, **140**, 6631–6642.
131 R. A. Dragovic, C. Gardiner, A. S. Brooks, D. S. Tannetta, D. J. Ferguson, P. Hole, B. Carr, C. W. Redman, A. L. Harris, P. J. Dobson, P. Harrison and I. L. Sargent, *Nanomedicine*, 2011, **7**, 780–788.
132 D. D. Taylor and S. Shah, *Methods*, 2015, **87**, 3–10.
133 Z. Wang, H.-J. Wu, D. Fine, J. Schmulen, Y. Hu, B. Godin, J. X. Zhang and X. Liu, *Lab Chip*, 2013, **13**, 2879–2882.
134 S. M. Santana, M. A. Antonyak, R. A. Cerione and B. J. Kirby, *Biomed. Microdevices*, 2014, **16**, 869–877.
135 B. H. Wunsch, J. T. Smith, S. M. Gifford, C. Wang, M. Brink, R. L. Bruce, R. H. Austin, G. Stolovitzky and Y. Astier, *Nat. Nanotechnol.*, 2016, **11**, 936–940.
136 A. Leshansky, A. Bransky, N. Korin and U. Dinnar, *Phys. Rev. Lett.*, 2007, **98**, 234501.
137 C. Liu, J. Guo, F. Tian, N. Yang, F. Yan, Y. Ding, J. Wei, G. Hu, G. Nie and J. Sun, *ACS Nano*, 2017, **11**, 6968–6976.
138 R. T. Davies, J. Kim, S. C. Jang, E.-J. Choi, Y. S. Gho and J. Park, *Lab Chip*, 2012, **12**, 5202–5210.
139 S. Cho, W. Jo, Y. Heo, J. Y. Kang, R. Kwak and J. Park, *Sens. Actuators, B*, 2016, **233**, 289–297.
140 F. Liu, O. Vermesh, V. Mani, T. J. Ge, S. J. Madsen, A. Sabour, E.-C. Hsu, G. Gowrishankar, M. Kanada, J. V. Jokerst, R. G. Sierra, E. Chang, K. Lau, K. Sridhar, A. Bermudez, S. J. Pitteri, T. Stoyanova, R. Sinclair, V. S. Nair, S. S. Gambhir and U. Demirci, *ACS Nano*, 2017, **11**, 10712–10723.
141 H. Bruus, J. Dual, J. Hawkes, M. Hill, T. Laurell, J. Nilsson, S. Radel, S. Sadhal and M. Wiklund, *Lab Chip*, 2011, **11**, 3579–3580.
142 L. Y. Yeo and J. R. Friend, *Annu. Rev. Fluid Mech.*, 2014, **46**, 379–406.
143 K. Lee, H. Shao, R. Weissleder and H. Lee, *ACS Nano*, 2015, **9**, 2321–2327.
144 J. C. Giddings, *Science*, 1993, **260**, 1456–1466.
145 S. Oh, D. Kang, S. M. Ahn, R. J. Simpson, B. H. Lee and M. H. Moon, *J. Sep. Sci.*, 2007, **30**, 1082–1087.
146 D. Kang, S. Oh, S.-M. Ahn, B.-H. Lee and M. H. Moon, *J. Proteome Res.*, 2008, **7**, 3475–3480.
147 J. S. Yang, J. C. Lee, S. K. Byeon, K. H. Rha and M. H. Moon, *Anal. Chem.*, 2017, **89**, 2488–2496.
148 K. E. Petersen, E. Manangon, J. L. Hood, S. A. Wickline, D. P. Fernandez, W. P. Johnson and B. K. Gale, *Anal. Bioanal. Chem.*, 2014, **406**, 7855–7866.
149 S. D. Ibsen, J. Wright, J. M. Lewis, S. Kim, S.-Y. Ko, J. Ong, S. Manouchehri, A. Vyas, J. Akers, C. C. Chen, B. S. Carter, S. C. Esener and M. J. Heller, *ACS Nano*, 2017, **11**, 6641–6651.
150 J. M. Lewis, A. D. Vyas, Y. Qiu, K. S. Messer, R. White and M. J. Heller, *ACS Nano*, 2018, **12**, 3311–3320.
151 C. Chen, J. Skog, C.-H. Hsu, R. T. Lessard, L. Balaj, T. Wurdinger, B. S. Carter, X. O. Breakefield, M. Toner and D. Irimia, *Lab Chip*, 2010, **10**, 505–511.
152 S. S. Kanwar, C. J. Dunlay, D. M. Simeone and S. Nagrath, *Lab Chip*, 2014, **14**, 1891–1900.
153 P. Zhang, M. He and Y. Zeng, *Lab Chip*, 2016, **16**, 3033–3042.
154 J. S. Dudani, D. R. Gossett, H. T. Tse, R. J. Lamm, R. P. Kulkarni and D. D. Carlo, *Biomicrofluidics*, 2015, **9**, 014112.
155 J. Rho, J. Chung, H. Im, M. Liong, H. Shao, C. M. Castro, R. Weissleder and H. Lee, *ACS Nano*, 2013, **7**, 11227–11233.
156 D. Issadore, C. Min, M. Liong, J. Chung, R. Weissleder and H. Lee, *Lab Chip*, 2011, **11**, 2282–2287.
157 M. He, J. Crow, M. Roth, Y. Zeng and A. K. Godwin, *Lab Chip*, 2014, **14**, 3773–3780.
158 Z. Zhao, Y. Yang, Y. Zeng and M. He, *Lab Chip*, 2016, **16**, 489–496.
159 K. Ueda, N. Ishikawa, A. Tatsuguchi, N. Saichi, R. Fujii and H. Nakagawa, *Sci. Rep.*, 2014, **4**, 6232.
160 R. Vaidyanathan, M. Naghibosadat, S. Rauf, D. Korbie, L. G. Carrascosa, M. J. Shiddiky and M. Trau, *Anal. Chem.*, 2014, **86**, 11125–11132.
161 H. Im, H. Shao, Y. I. Park, V. M. Peterson, C. M. Castro, R. Weissleder and H. Lee, *Nat. Biotechnol.*, 2014, **32**, 490–495.
162 L. Zhu, K. Wang, J. Cui, H. Liu, X. Bu, H. Ma, W. Wang, H. Gong, C. Lausted and L. Hood, *Anal. Chem.*, 2014, **86**, 8857–8864.
163 D. L. Rupert, C. Lässer, M. Eldh, S. Block, V. P. Zhdanov, J. O. Lotvall, M. Bally and F. Höök, *Anal. Chem.*, 2014, **86**, 5929–5936.
164 A. A. I. Sina, R. Vaidyanathan, S. Dey, L. G. Carrascosa, M. J. Shiddiky and M. Trau, *Sci. Rep.*, 2016, **6**, 30460.
165 R. Lacroix, S. Robert, P. Poncelet, R. Kasthuri, N. Key and F. Dignat-George, *J. Thromb. Haemostasis*, 2010, **8**, 2571–2574.

166 C. F. Bohren and D. R. Huffman, *Absorption and scattering of light by small particles*, John Wiley & Sons, 2008.
167 E. Van Der Pol, M. Van Gemert, A. Sturk, R. Nieuwland and T. Van Leeuwen, *J. Thromb. Haemostasis*, 2012, **10**, 919–930.
168 E. J. Van Der Vlist, E. N. Nolte, W. Stoorvogel, G. J. Arkesteijn and M. H. Wauben, *Nat. Protoc.*, 2012, **7**, 1311.
169 V. Pospichalova, J. Svoboda, Z. Dave, A. Kotrbova, K. Kaiser, D. Klemova, L. Ilkovics, A. Hampl, I. Crha, E. Jandakova, L. Minar, V. Weinberger and V. Bryja, *J. Extracell. Vesicles*, 2015, **4**, 25530.
170 A. Morales-Kastresana, B. Telford, T. A. Musich, K. McKinnon, C. Clayborne, Z. Braig, A. Rosner, T. Demberg, D. C. Watson, T. S. Karpova, G. J. Freeman, R. H. DeKruyff, G. N. Pavlakis, M. Terabe, M. Robert-Guroff, J. A. Berzofsky and J. C. Jones, *Sci. Rep.*, 2017, **7**, 1878.
171 L. Löf, T. Ebai, L. Dubois, L. Wik, K. G. Ronquist, O. Nolander, E. Lundin, O. Söderberg, U. Landegren and M. Kamali-Moghaddam, *Sci. Rep.*, 2016, **6**, 34358.
172 O. Söderberg, M. Gullberg, M. Jarvius, K. Ridderstråle, K.-J. Leuchowius, J. Jarvius, K. Wester, P. Hydbring, F. Bahram and L.-G. Larsson, *Nat. Methods*, 2006, **3**, 995–1000.
173 E. Pol, F. Coumans, A. Grootemaat, C. Gardiner, I. Sargent, P. Harrison, A. Sturk, T. Leeuwen and R. Nieuwland, *J. Thromb. Haemostasis*, 2014, **12**, 1182–1192.
174 F. Gao, Y. Cui, H. Jiang, D. Sui, Y. Wang, Z. Jiang, J. Zhao and S. Lin, *Oncotarget*, 2016, **7**, 71330–71340.
175 M. Yu, A. Bardia, N. Aceto, F. Bersani, M. W. Madden, M. C. Donaldson, R. Desai, H. Zhu, V. Comaills, Z. Zheng, B. S. Wittner, P. Stojanov, E. Brachtel, D. Sgroi, R. Kapur, T. Shioda, D. T. Ting, S. Ramaswamy, G. Getz, A. J. Iafrate, C. Benes, M. Toner, S. Maheswaran and D. A. Haber, *Science*, 2014, **345**, 216–220.
176 E. Ozkumur, A. M. Shah, J. C. Ciciliano, B. L. Emmink, D. T. Miyamoto, E. Brachtel, M. Yu, P.-i. Chen, B. Morgan, J. Trautwein, A. Kimura, S. Sengupta, S. L. Stott, N. M. Karabacak, T. A. Barber, J. R. Walsh, K. Smith, P. S. Spuhler, J. P. Sullivan, R. J. Lee, D. T. Ting, X. Luo, A. T. Shaw, A. Bardia, L. V. Sequist, D. N. Louis, S. Maheswaran, R. Kapur, D. A. Haber and M. Toner, *Sci. Transl. Med.*, 2013, **5**, 179ra47.